Inhibitory Control and Integration in the Thalamus

PhD Dissertation

Viktor Plattner

János Szentágothai Doctoral School of Neurosciences
Semmelweis University

Supervisor:	László Acsády, DSc
Official Reviewers:	Magor Lőrincz, Ph.D Anita Kamondi, MD, DSc
Head of the Final Examination Committee:	Béla Halász, MD, DSc
Members of the Final Examination Committee:	György Karmos, MD, CSc Bence Rácz, Ph.D

Budapest
2016

Table of Contents

Table of Contents i

List of Abbreviations iv

1 Introduction 1

1.1 Thalamus – the classical view 1

1.2 Connectional diversity of thalamic nuclei – the intralaminar group 2

1.3 Functional overview of the intralaminar nuclei 4

1.4 Afferents of the intralaminar nuclei 6

1.5 Inhibitory inputs in the thalamus 7

1.6 Glycinergic neurotransmission – novel sources of inhibition in the forebrain 9

1.7 Integration in the thalamus 11

1.8 Key points of the introduction 13

2 Objectives 14

3 Methods 15

3.1 Animal housing and treatement 15

3.2 Processing of human samples 15

3.3 Used transgenic animal strains 15

3.3.1 GlyT2::eGFP mouse line 15

3.3.2 GlyT2::cre mouse line 16

3.3.3 GlyT2::eGFP/Rbp4::cre mouse line 16

3.4 Morphology 16

3.4.1 Surgery 16

3.4.2 Standard procedure for immunohistochemistry and standard incubation times 17

3.4.3 Retrograde tracing and immunohistochemistry 19

3.4.4 Anterograde tracing and immunohistochemistry 20

3.4.5 Electron microscopy 23

3.4.6 Human tissues preparation 24

3.5 In vivo physiology 25

3.5.1 Surgery 25

3.5.2 In vivo juxtacellular recording and labeling, local field potential (LFP) recording 25

3.5.3 Analysis 26

3.5.4 In-vivo optogenetics and LFP recordings 27

4 Results 30

Part I – Novel source of inhibition in the thalamus 30

4.1 Distribution of glycinergic fibers in the thalamus, retrograde tracing, origin of the pathway 30

4.2 Activity of glycinergic neurons in anaesthetized animals 34

4.3 Activation of the pathway, effects on thalamic neurons 39

4.4 Activation of the pathway in freely moving animals 43

4.5 Cortico-PRF Pathway 48

4.6 Spontaneus desynchronization, pharmacological inactivation 51

4.7 Electrical and optical activation 54

Part II – Integration in the thalamus 57

4.8 Integration in the thalamus - convergence of driver inputs on a single TC neuron 57

5 Discussion 62

5.1 Technical considerations 62

5.2 A novel source of inhibition in the thalamus 62

5.3 Cortical control of the extrathalamic system 65

5.4 Participation of the intralaminar thalamus in various tasks 66

5.5 Integration in the thalamus 67

6 Conclusions 69

6.1 Short- and mid-term goals 69

6.2 Perspectives 69

Summary 71

Összefoglalás 72

Bibliography 73

Bibliography of the candidate's publications 79

Acknowledgements **80**

List of Figures **81**

List of Abbreviations

ABC	avidin biotin peroxidase complex
AP	action potential
APT	anterior pretectum
BAC	bacterial artificial chromosome
BDA	biotinylated dextrane amine
BSA	bovine serum albumin
CB	calbindin
CeM	central medial nucleus of the thalamus
Cg	cingulate cortex
ChR2	channel rhodopsin 2
CL	centrolateral nucleus of the thalamus
CM	center median nucleus of the thalamus
CRS - R	Coma Recovery Scale – Revised
CSD	cortical spreading depression
DAB	diaminobenzidine
DAB-Ni	nickel intensified diamino benzidine
DBS	deep brain stimulation
DNA	deoxyribonucleic acid
EEG	electroencephalogram
eGFP	enhanced green fluorescent protein
EM	electron microscopy
EPSP	excitatory postsynaptic potential
FG	fluorogold
FR	firing rate
GABA	gamma amino butyric acid
GlyT1	type 1 glycine transporter

GlyT2	type 2 glycine transporter
IL	intralaminar thalamic nuclei
IPSC	inhibitory postsynaptic current
ISI	inter spike interval
KCl	potassium chloride
L5	layer 5 of the cerebral cortex
L6	layer 6 of the cerebral cortex
LCN	lateral cerebellar nucleus
LFP	local field potential
LTD	long term depression
LTP	long term potentiation
M2	secondary motor cortex
MCS	minimal conscious state
MD	mediodorsal nucleus of the thalamus
MFR	mean firing rate
MUA	multiunit activity
NMDA	N-methyl-D-aspartate receptor
PB	phosphate buffer
PC	paracentral nucleus of the thalamus
Pf	parafascicular nucleus of the thalamus
PHAL	Phaseolus vulgaris leucoagglutinin
PnC	nucleus pontis caudalis
PnO	nucleus pontis oralis
POm	posterior nucleus of the thalamus
PRF	pontine reticular formation
PSTH	peristimulus time histogram
Rbp4	retinol binding protein 4

RDP	Rapid onset dystonia-Parkinsonism
ROI	region of interest
S1	primary somatosensory cortex
SNr	substantia nigra pars reticulata
STA	spike triggered average
SWS	slow wave sleep
TBS	tris-buffered saline
TC	thalamocortical
Thy1	thymus cell antigen 1
TRN	thalamic reticular nucleus
VA	ventral anterior nucleus of the thalamus
vGAT	vesicular GABA transporter
vGluT1	type 1 vesicular glutamate transporter
vGluT2	type 2 vesicular glutamate transporter
vIAAT	vesicular inhibitory amino acid transporter
VL	ventrolateral nucleus of the thalamus
VM	ventromedial nucleus of the thalamus
VPM	ventral posteromedial nucleus of the thalamus
Zi	zona incerta

1 Introduction

The thalamus is situated between the highly developed cerebral cortex and the evolutionarily older hindbrain structures. In primates its two sides are only connected by the *adhesio interthalamica*, while in rodents they are united. The thalamus is the largest area of the diencephalon, and it has two parts with developmentally different origins. One is the dorsal thalamus that includes the cortical-projecting thalamic nuclei, and it is generally refered to as thalamus. The other is the ventral thalamus that holds the GABAergic (gamma amino butyric acid) cells of the thalamic reticular nucleus (TRN), which play a key role in thalamocortical oscillation genesis (Barthó et al., 2014). The main cell type of the thalamus is called - for historical reasons - the *thalamic relay cell* or, based on a more recent terminology, the *thalamocortical* (TC) cell. In this thesis I will refer to thalamic neurons either as relay cells or as TC neurons depending on their connectivity and role in information transmission.

1.1 Thalamus – the classical view

-According to the classical view, the thalamus serves as a relay station for ascending sensory information arriving from sensory organs that then travels on towards the cerebral cortex for processing- (Le Gros Clark, 1932; A. Earl Walker and Walker, 1936; Walker, 1938). Thus, its only role was thought to be the faithful transmission of these sensory messages without failure or modification. Several thalamic nuclei certainly fullfill this role. These nuclei receive their main excitatory „driver" (Sherman and Guillery, 1998, 2001; Guillery and Sherman, 2002; Bickford, 2015) input from sensory subcortical areas, and send their axons to layer 4 of a specific cortical region with well defined function (Fig. 1.2.1 a) (Herkenham, 1980; Jones, 2007; Clascá et al., 2012, 2016). Based on the terminology of Sherman and Guillery, we can refer to these regions as *first order* nuclei (Sherman and Guillery, 2001). For a long time, these nuclei served as the model of the organization principle of thalamocortical connectivity, and the classical view of the thalamus was generalized from their properties. Besides their innervation and projection pattern within these regions, both the morphological and physiological features of relay cells

and sensory axons indeed support faithful information transmission. Fibers carrying sensory information target the thick proximal domain of relay cell dendrites and form large glutamatergic driver terminals with multiple release sites (Sherman and Guillery, 2001; Bickford, 2015). These terminals display high initial release probability and evoke fast-rising excitatory postsynaptic potentials (EPSP) with large amplitude (Sherman and Guillery, 1998; Deschenes et al., 2003). Repetitive activation of these inputs results in frequency-dependent depression of the postsynaptic response (Bickford, 2015).

1.2 Connectional diversity of thalamic nuclei – the intralaminar group

-*Although these properties are true for severeal thalamic nuclei, many others do not fit in this classical framework i.e. the rule of faithful transfer of sensory messages to specific cortical areas is not universal.*-(Sherman and Guillery, 2001). The majority of thalamic regions show an entirely different organization and connection pattern with the cortex, both in terms of afferents and efferents (Herkenham, 1980; Sherman and Guillery, 1996; Clascá et al., 2012, 2016). Part of them do not follow the strict topography and point-to-point projection of those relaying sensory information. Instead, their efferents target large and widespread cortical regions or specifically innervate multiple areas, and the laminar distribution of the axons also shows great variability (Fig. 1.2.1 b, c) (for review see Clascá *et al.*, 2012, 2016).

Moreover, the „driver" afferents in particular thalamic nuclei are not classical either, in the sense that they have cortical origin. Thus they putatively convey a message fundamentally different from sensory information. In contrast to the previously mentioned *first order* regions, we can refer to these parts of the thalamus as *higher order* areas.

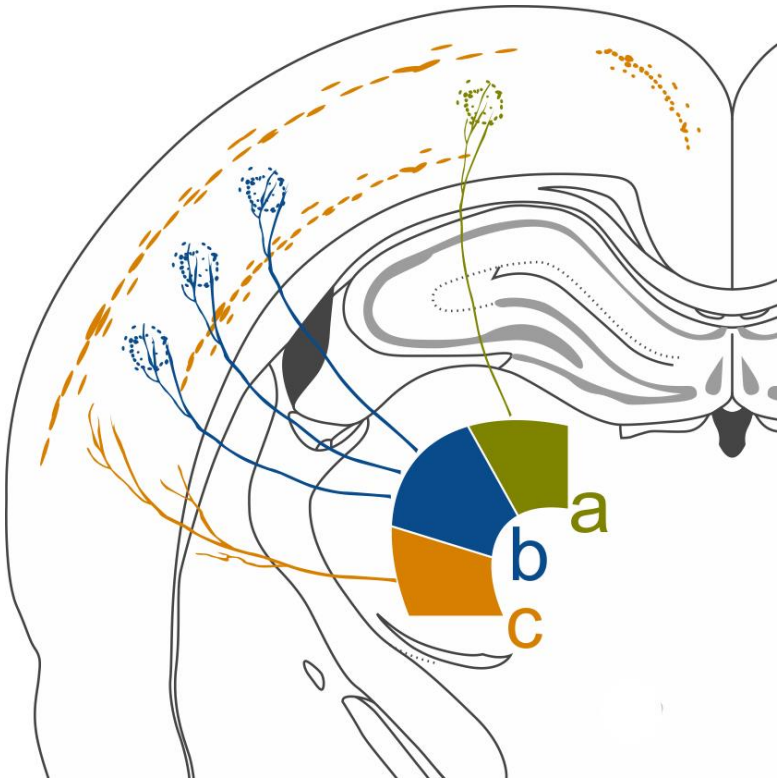

Figure 1.2.1. Example of different projection patterns of various thalamic nuclei.

a) Specific projection from the thalamus to a well defined cortical region. **b)** Multispecific projection from the thalamus to the cortex. TC neurons innervate several distinct well defined cortical regions. **c)** Thalamic projection to large cortical areas and to subcortical structures (e.g. striatum).

Some thalamic nuclei also innervate subcortical targets, making them potential hubs connecting command organizer and executor networks (Sherman and Guillery, 2001; Jones, 2007; Clascá et al., 2016). The intralaminar (IL) complex is a group of thalamic nuclei that have a vast frontal cortical projection and also extensively innervate the striatum (Van der Werf et al., 2002; Clascá et al., 2016). The group is situated within the internal medullary lamina and consists of numerous nuclei. The anterior intralaminar group includes the *central medial* (CeM), the *paracentral* (Pc) and the *central lateral* (CL) nuclei, while the posterior intralaminar group holds the *center median – parafascicular* (CM-Pf) nuclei (separated only in primates). They have different projection patterns, both in the cortex and in the striatum

(Van der Werf et al., 2002). In accordance with the variety of their efferents, these nuclei show great functional diversity as well.

1.3 Functional overview of the intralaminar nuclei

-*IL nuclei play diverse roles in several brain functions.*- These roles are, although seemingly different, not necessarily conflicting. Numerous experiments and human case studies indicate that IL nuclei have a prominent effect on consciousness and awareness (Kinney et al., 1994; Schiff et al., 2007). Others discuss that their activity affects the sleep-wake cycle and arousal (Hunter and Jasper, 1949); still others explain their role in motor functions (Chen et al., 2014; Rodriguez-Sabate et al., 2014), and there are examples of their participation in learning and memory consolidation (Bradfield et al., 2013; Pereira de Vasconcelos and Cassel, 2015). Based on their connectivity, all of the above are plausible.

IL nuclei act like a hub in the communication between the brainstem and the forbrain, and severe cognitive disfunction can be observed if they are damaged. Their importance is supported by the case of Karen Ann Quinlan (Kinney et al., 1994) who, after a cardiopulmonary arrest, fell into a persistent vegetative state. She was unable to communicate and did not show any signs of awareness, although her sleep wake cycle remained intact. The *post mortem* examination of her brain revealed that, contrary to the expectations, the cerebral cortex was not seriously damaged. Cortical scars could only be observed in the occipital pole and the parasagittal parieto-occipital region. Different components of the ascending activating system, including the brainstem, basal forebrain and hypothalamus, were also undamaged. However, in the whole thalamus, including the IL nuclei, severe cell loss could be detected. The damage was not uniform in the IL. The centrolateral and paracentral nuclei were strongly affected, as well as the centromedial nucleus, while the cell loss in the parafascicular nucleus was moderate compared to the others. These findings demonstrate that the IL nuclei can play a complex role in cognitive functions.

In accordance with these observations, the electrical stimulation of the IL nuclei was shown to improve arousal state, communication abilities and motor functions in a patient who remained in minimal conscious state (MCS) after a traumatic brain injury (Schiff et al., 2007).

In MCS, large scale cortical networks can be preserved, suggesting the possibility of partial functional recovery. After implanting two stimulating electrodes bilaterally to the thalamus targeting the CL and the CM-Pf complex, numerous tests were performed to tune the optimal stimulation parameters. To assess the effects of DBS, behavior and responsiveness were monitored in three categories. Results were evaluated by the so called JFK Coma Recovery Scale – Revised (CRS – R), which is a validated method used to measure neurobehavioural functions. The overall state of arousal was increased and the previously non-responsive patient showed dramatic improvements in communication, limb control and oral feeding compared to the presurgical baseline. Together with the previous case study, these results endorse the role of IL nuclei in cognitive functions.

Other studies raise the possibility of IL playing a role in the organization of the sleep-wake cycle. In 1949, Hunter and Jasper studied the effects of electrical stimulation of the IL nuclei in freely moving cats (Hunter and Jasper, 1949). They delivered 25 ms-long square wave pulses at 3-5 Hz and observed an increased response threshold to sensory stimulation, and detected rhythmic spindles and slow waves in the cortical EEG. In this study, depending on the parameters of the electrical stimulation, the authors also discovered movement-related effects. In the case of moderate intensities, bilateral twitching movements of the face, and in the case of higher intensities and lower frequencies (2-4 Hz) bilateral clonic movements of the face, forelimbs and body were observed. At higher intensities, tonic elevation of one forepaw and contralateral turning movements occured, but according to the authors, in these cases the stimulus might have not been specific to the IL nuclei.

Planning and executing complex movements requires proper communication of cerebral cortical motor centers, the basal ganglia and the cerebellum. As previously mentioned, the IL nuclei project to the striatum, the first station of the basal ganglial circuit directly innervated by the cortex. Rodriguez-Sabate and co-workers showed functional connectivity of IL nuclei with all basal ganglia in humans during resting state and in motor tasks using the correlation of BOLD signals (Rodriguez-Sabate et al., 2014). They concluded that IL thalamus influenced the strength of the functional connectivity of the striatum with other

basal ganglia so it was not only critical for striatal activity but also for the normal operation of the whole basal ganglia network.

Via the intralaminar thalamus, cerebellar information can also enter this circuit. The lateral cerebellar nucleus (LCN) was shown to innervate the striatum-projecting CL neurons (Ichinohe et al., 2000; Chen et al., 2014). The functional relevance of this disynaptic pathway was described by Chen and colleagues (Chen et al., 2014). They showed that the cerebellum can rapidly modulate striatal activity and cortico-striatal plasticity via the CL. The connection between striatum and the cerebral cortex is essential in motor learning, and the plasticity of this synapse has been shown earlier (Calabresi et al., 1992a, 1992b; Charpier and Deniau, 1997). After high frequency activation of the cortico-striatal pathway, the synapse on striatal neurons showed long term depression (LTD) that could be turned into long term potentiation (LTP) with the concurrent activation of the cerebellum. They also demonstrated the function of this pathway under pathological conditions. Rapid onset dystonia-Parkinsonism (RDP) is caused by the propagation of aberreant cerebellar activity to the basal ganglia via the IL (Calderon et al., 2011). They showed that in pharmacologically induced RDP, the propagation of altered cerebellar activity to the striatum could be prevented by either electrical lesion or optical inactivation of the IL.

Others observed damage to the IL-striatal pathway in Parkinson's disease. Morales and colleagues showed that increased striatal glutamate can cause retrograde cell degeneration, not only in the dopaminergic cells of the substantia nigra but also in the striatum-projecting IL neurons (Morales et al., 2013). This retrograde excitotoxicity can play a role in the development of Parkinson's disease.

1.4 Afferents of the intralaminar nuclei

According to the studies described above it is clear that IL nuclei participate in many tasks different from sensory information transmission, and from their cortical projection pattern and subcortical connections we can notice that they do not fit in the classical model of thalamocortical organization. -*But is it only their output that makes them peculiar, or do they receive different input as well?*- Some of the afferents arriving to the IL

are shared among nuclei, but there are certain differences between their innervation. As partially mentioned previously, IL nuclei act like a communication channel between brainstem and forebrain. Accordingly, a massive innervation arrives from different brainstem nuclei, especially from the components of the reticular activating system (Van der Werf et al., 2002). A serotonergic projection from the raphe and noradrenergic fibers from the locus coeruleus can be found in all IL nuclei, while cholinergic innervation from the pedunculopontine and laterodorsal tegmental nuclei is typically found in the CM (Van der Werf et al., 2002). The supramamillary nucleus also innervates the IL complex, and topographic projections from different layers of the superior colliculus and from different sectors of the periaqueductal gray matter can also be observed (Krout and Loewy, 2000; Krout et al., 2001; Van der Werf et al., 2002). The lateral cerebellar nucleus (LCN) also sends fibers to the striatum-projecting CL neurons (Ichinohe et al., 2000). The importance of this projection was described in the functional overview (Chen et al., 2014).

The great variety of inputs arriving to the IL, as well as the diversity of projections, raises the possibility of the IL being more than a relay station that faithfully transmits incoming information. It seems to act more like a hub, receiving subcortical modulatory inputs and several other types of messages from multiple sources, having access both to cortical areas and, via the striatum, to the movement-organizing basal ganglial circuit.

1.5 Inhibitory inputs in the thalamus

As it was demonstrated, thalamic nuclei like the IL complex show great variability in terms of projection pattern and excitatory afferents, so the classical anatomical and functional generalization of thalamocortical networks is not appropriate. -*So far, only excitatory inputs of the thalamus were described, but no biological system can be stable without inhibition.*- In the thalamus, the general source of this inhibition is the GABAergic cells of the thalamic reticular nucleus (TRN) (Jones, 1985). This shell-like structure covers the ventral anterior side of the thalamus and forms point-to-point reciprocal connection with all of its nuclei. TRN terminals target every functional domain of the thalamic cells, from the soma to the very distal dendritic regions, and exhibit a tonic

hyperpolarizing effect via small sized terminals with one or occasionally two active zones. The result of this hyperpolarization and the co-operation of T-type calcium and H-type channels is the burst activity of thalamic neurons observed during sleep (Jahnsen and Llinás, 1984). The connectivity and rhythmic interaction of the thalamus and the TRN is the basis of spindle genesis and thalamocortical oscillatory activity (Barthó et al., 2014).

-In particular thalamic nuclei, inhibitory inputs from extrathalamic sources are also present.- Higher order thalamic regions, as well as the presented IL nuclei, are innervated by the GABAergic fibers of the zona incerta (Zi) (Bartho et al., 2002), the anterior pretectum (APT) (Bokor et al., 2005) and the substantia nigra pars reticulata (SNr) (Bodor et al., 2008). Incertal fibers were found in the largest density in the posterior thalamic nucleus (POm), in the lateral parts of the ventrolateral thalamic nuclei and in several IL nuclei (Bartho et al., 2002). APT-thalmic fibers also targeted all higher order nuclei, and the CL and mediodorsal (MD) nuclei of the IL complex (Bokor et al., 2005), while nigral terminals could be observed in the ventral anterior (VA), ventrolateral (VL), ventromedial (VM) and also in the intralaminar nuclei (Bodor et al., 2008).

Extrathalamic inhibitory fibers not only show preference for distinct thalamic nuclei, but also for specific functional domains of the TC neurons, targeting their thick proximal dendrites with large terminals containing multiple release sites (Bartho et al., 2002; Bokor et al., 2005; Bodor et al., 2008). In contrast to the tonic effect of TRN, the functional consequences of these morphological properties are fast transient postsynaptic inhibitory currents. In the case of the APT-thalamic connection, it was shown that inhibitory responses could be evoked with very short latency and small jitter. Also, paired pulse activation revealed the non-depressing nature of the synapse (Bokor et al., 2005). Fast transient extrathalamic inhibition can effectively regulate the firing of TC neurons and the propagation of excitation into the soma in specific cases (Lavallée et al., 2005).

1.6 Glycinergic neurotransmission – novel sources of inhibition in the forebrain

The possibility of the existence of additional extrathalamic inhibitory pathways besides the presented ones was raised after a paper published by Zeilhofer and colleagues in 2005 (Zeilhofer et al., 2005). They created a type 2 glycine transporter (GlyT2)::enhanced green fluorescent protein (eGFP) transgenic mouse line expressing eGFP in glycinergic neurons. In the midbrain of these animals a strong fluorescent signal could be observed emitted by a profuse network of axons and terminals (Fig. 1.6.1).

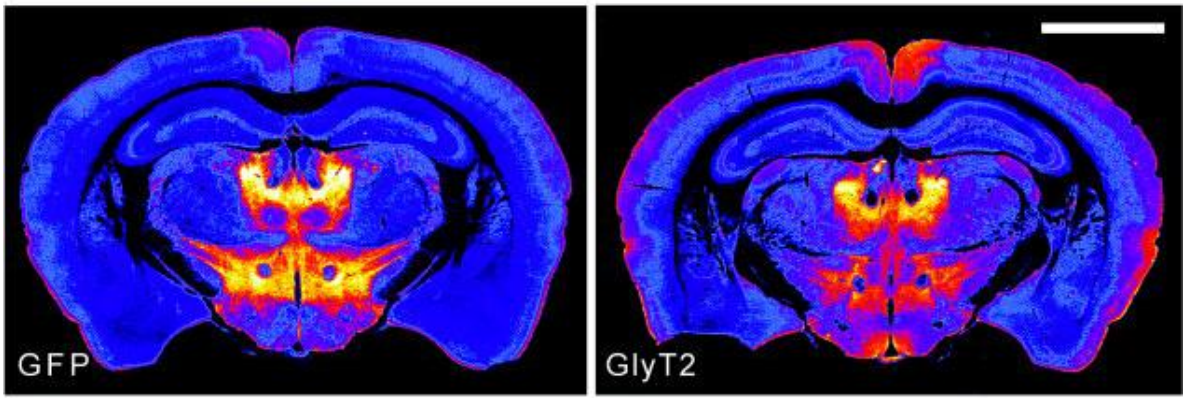

Figure 1.6.1. Glycinergic labelling in the midbrain of GlyT2::eGFP transgenic animals. GFP signal in a GlyT2::eGFP transgenic animal (left). GlyT2 immunoreaction (right). Note the overlap between the intrinsic eGFP signal and immunolabeling (Modified from Zeilhofer *et al*., 2005).

Glycine is the simplest proteinogenic amino acid. The discovery of its high concentration in the spinal cord and in the brainstem in the 1960's raised the possibility of its potential role as a neurotransmitter (for review see: Bowery and Smart, 2006; Hernandes and Troncone, 2009). Glycinergic neurotransmission has been known to be common in the these areas since the early 1970's (for review see Bowery and Smart, 2006).

The main source of glycine is the serine-glycine metabolic pathway, catalyzed by glycine decarboxylase and serine hydroxymethyltransferase. To act as a neurotransmitter, glycine needs to be first accumulated in the synaptic terminals and then in the synaptic vesicles. The former is achieved by the GlyT2 molecule being expressed by glycinergic neurons (in

contrast to the type 1 glycine transporter (GlyT1) molecule, which is a glia-specific transporter) (Liu et al., 1993), while the latter is performed by the vesicular inhibitory amino acid transporter (vIAAT, also known as vesicular GABA transporter - vGAT), the co-transporter of glycine and GABA (McIntire et al., 1997; Sagné et al., 1997; Wojcik et al., 2006).

Although the potential role of glycine as a neurotransmitter was suggested earlier, the glycine receptor was only isolated in 1983. These receptors are built from alpha and beta subunits, and in adult tissue 2α and 3β subunits form a heteropentameric transmembrane ion channel. Upon glycine binding, a pore opens that selectively allows Cl^- ions to flow across the membrane, causing hyperpolarization of the membrane potential. The inhibitory effect of glycine is fundamental for voluntary motor control, for spinal inhibitory reflexes allowing the relaxation of antagonistic muscles, and is also involved in cardiovascular, auditory and respiratory functions (for review see: Bowery and Smart, 2006; Hernandes and Troncone, 2009).

During developement, when the intracellular Cl^- ion concentration is increased in several parts of the brain, glycine and GABA have a depolarizing effect, and thus act as an excitatory transmitter. This is believed to be important for neuronal differentiation and synaptogenesis. In the mature nervous system, glycine is also needed for the activation of N-methyl-D-aspartate (NMDA) receptors. NMDA receptors have a glutamate/aspartate and a glycine/serine binding site, and both of these have to be occupied to activate the ion channel. The concentration of glycine in the glutamatergic synaptic cleft may be regulated by the GlyT1-expressing glial cells (for review see: Hernandes and Troncone, 2009).

1.7 Integration in the thalamus

Throughout the previous sections, I presented examples of how the diversity of thalamic afferents and projection patterns make the picture of thalamocortical operation more complex, but I did not talk about how thalamic regions receiving afferents from various sources deal with the incoming information, and what may happen to that information at the level of the thalamus.

In particular thalamic nuclei, besides the classical subcortical sensory drivers, other terminals that share the morphological and physiological properties of a driver (large terminals with multiple active zones, fast excitatory postsynaptic potentials (EPSP) with large amplitude) can also be observed. These terminals are known to have L5 cortical origin and innervate the exact same proximal dendritic domain of TC cells as inputs coming from subcortical sources (Sherman and Guillery, 1996, 2001; Bickford, 2015). As it was mentioned before, thalamic regions receiving only subcortical drivers and relaying sensory information to a specific sensory cortical area are called *first order* nuclei, while the those innervated by cortical drivers are named *higher order* nuclei (Sherman and Guillery, 2001). The distribution of driver terminals with different origin was mapped in the whole primate thalamus (Rovó et al., 2012) using the type I vesicular glutamate transporter (vGluT1) as a marker of cortical terminals and the type II vesicular glutamate transporter (vGluT2) as a marker of subcortical terminals. The study revealed that in some thalamic regions these inputs were completely separated, while in others they colocalized, but that areas entirely lacking driver terminals also existed (Fig. 1.7.1).

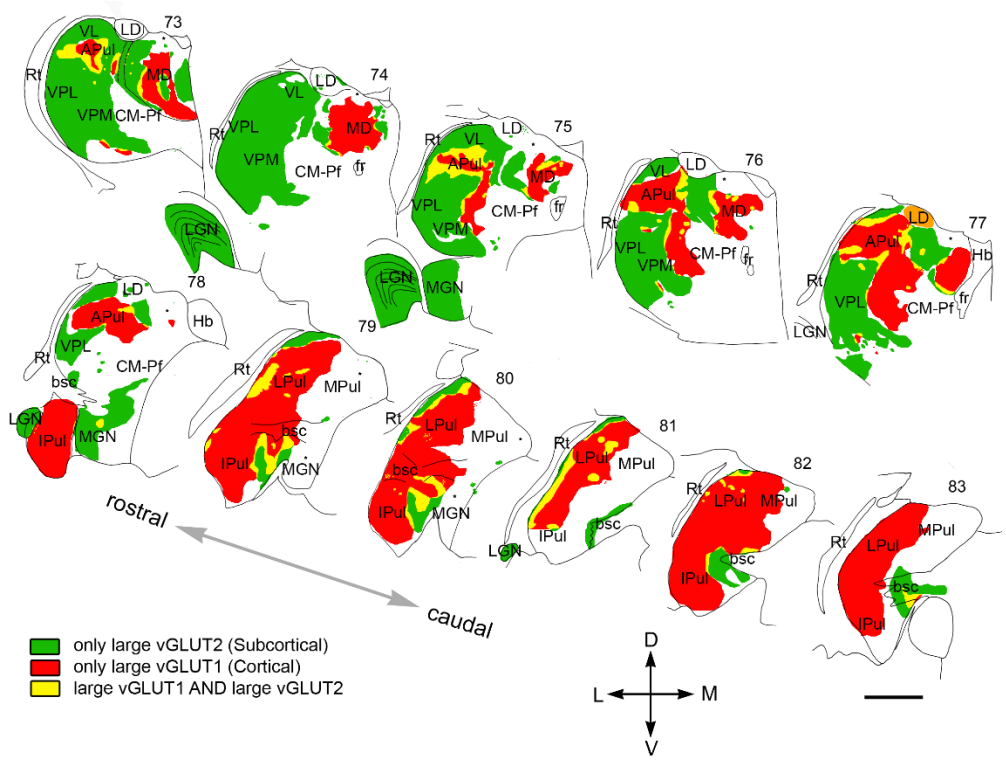

Figure 1.7.1. Distribution of drivers with different origin in the primate thalamus. (Modified from Rovó *et al*., 2012).

It is important to note here that vGluT1 labels axons from both layer 5 (L5) and layer 6 (L6) of the cerebral cortical pyramidal cells. These two can easily be differentiated by their morphological properties (number of release sites, postsynaptic target domain) (Jones, 2007; Bickford, 2015) and by their physiological effect (rise time and amplitude of the evoked EPSP). L6 of the cerebral cortex innervates all thalamic cells and serves as a modulatory input, tuning the activity and sensitivity of TC neurons (Sherman and Guillery, 2001).

-The colocalization of driver terminals with different origin in the same thalamic area raises the possibility of their convergence on a single thalamic cell and suggests that the output of such a neuron will be determined by two entirely different messages.

1.8 Key points of the introduction

- *According to the classical view, the thalamus serves as a relay station for ascending sensory information.*
- *Several thalamic nuclei do not fit into this classical framework.*
- *IL nuclei show an entirely different organization and connection pattern with the cortex, and play diverse roles in several brain functions.*
- *It is not only their output that makes them peculiar, but they also receive a large variety of afferents.*
- *Thalamic nuclei, besides excitatory afferents, also receive inhibition from thalamic sources and particular ones from extrathalamic sources.*
- *The possibility of the existence of a novel glycinergic extrathalamic inhibitory pathway was raised.*
- *The colocalization of driver terminals with different orgins raises the possibility of their convergence on a single thalamic cell, and thus the integrative role of particular thalamic regions.*

2 Objectives

The diversity of excitatory and inhibitory afferents in the thalamus, often in the same nuclei, as well as the heterogeneity of projection patterns and targeted cortical and subcortical areas, indicate that besides the well-described relay function of specific *first order* nuclei, a great part of the thalamus may play different roles in shaping information processing, and may also have complex executive functions.

In GlyT2::eGFP transgenic animals, our group discovered a massive cloud of glycinegic fibers targeting the IL complex, and found the possibility of convergence of excitatory driver inputs with different origin in the somatosensory thalamus of rodents.

In my PhD work for this thesis I have focused on two different aspects of thalamic activity control. First, I examined the role of *glycinergic inhibition* arriving to the IL complex in the regulation of motion. Second, I studied the convergence of *excitatory drivers* with different origin on the same TC cell.

My goals were:

1. To describe the glycinergic projection to the IL at the network and cellular levels, and to characterize the *in vivo* activity of the glycinergic cells.
2. To describe the effects of selective activation of the glycinergic pathway on IL activity and on the behavior of the animal.
3. To define the afferents of the glycinergic cells and the effect on their activity.
4. To show the putative integrative role of TC cells by characterizing the morphology of drivers with different origin converging onto the same neuron.

3 Methods

3.1 Animal housing and treatement

Mice were entrained to a 12 h light/dark cycle with food and water available *ad libitum*. All experimental procedures were performed according to the ethical guidelines of the Institute of Experimental Medicine of the Hungarian Academy of Sciences.

3.2 Processing of human samples

Human thalamic tissues (n = 3) were obtained from a male and two female patients (74, 59 and 76 years old, respectively). The subjects died from causes not linked to brain diseases, and none of them had a history of neurological disorders. The 3 subjects were processed for autopsy in Szent Borbála Hospital, Tatabánya, Department of Pathology. Informed consent was obtained for the use of their brain tissue for research purposes. Tissue was treated in a manner compliant with the Declaration of Helsinki. All performed procedures were approved by the Regional and Institutional Committee of Science and Research Ethics of the Scientific Council of Health (ETT TUKEB 31443/2011/EKU (518/PI/11)).

3.3 Used transgenic animal strains

3.3.1 GlyT2::eGFP mouse line

GlyT2 is a protein localized in the neuronal membrane and is responsible for capturing glycine molecules in the extracellular space and accumulating them inside the cell (Liu et al., 1993). Once the glycine reaches the proper intracellular concentration, the vIAAT molecule accumulates it in the synaptic vesicle, and thus it can function as an inhibitory neurotransmitter (McIntire et al., 1997; Sagné et al., 1997; Wojcik et al., 2006). GlyT2 is expressed in every glycinergic inhibitory neuron, making it their selective marker (Zafra et al., 1995).

In 2005, Zeilhofer and his colleagues created a reporter mouse strain in which eGFP was expressed under the control of the promoter of the GlyT2 gene, so glycinergic neurons showed green fluorescence (Zeilhofer et al., 2005). Performing the tracing experiments and

the juxtacellular recordings using these animals allowed us to *post hoc* identify the labeled neurons or fibers and the recorded units respectively.

3.3.2 GlyT2::cre mouse line

For the generation of this line, homologous recombination in bacteria was used to introduce the cre coding sequence into the BAC-DNA (bacterial artificial chromosome-deoxyribonucleic acid, clone RP23-365E4). The modified BAC-DNA was injected to the pronuclei of fertilized C57BL/6 oocytes. GlyT2::cre mouse lines were maintained on a C57BL/6J background. The selectivity of cre expression was demonstrated by performing immunostaining against the cre-protein (mouse anti-cre 1:10,000. Millipore, followed by Cy3-conjugated donkey anti-mouse 1:500) in crossed GlyT2::cre and GlyT2::eGFP mice. In these experiments, we examined 198 cre-positive neurons, out of which 196 (99%) were also eGFP-positive. We used these animals to selectively label glycinergic neurons using the cre-loxP system in gain of function experiments.

3.3.3 GlyT2::eGFP/Rbp4::cre mouse line

In these animals all glycinergic neurons show green fluorescence, and in addition cre recombinase is expressed in the cerebral cortex in layer 5 pyramidal neurons under the control of the promoter of the retinol binding protein 4 (Rbp4) gene. This double transgenic strain on the one hand allowed us to identify glycinergic neurons (as it was described previously in Chapter 3.3.1), and on the other hand to selectively label layer 5 pyramidal neurons in a cre-dependent manner.

3.4 Morphology

3.4.1 Surgery

Tracer and virus injections were performed under ketamine/xylazine anesthesia (ketamine, 83-111 mg/kg; xylazine, 3.3-4.3 mg/kg). The head of the animal was fixed in a stereotaxic apparatus (David Kopf Instruments, Tujunga, California 91042, Model 900 Small Animal

Stereotaxic Instrument). If needed, intramuscular injection of ketamine/xylazine was given to maintain anaesthesia.

3.4.2 Standard procedure for immunohistochemistry and standard incubation times

Fixation of the tissue: all animals, both for anatomical analysis and following acute or freely moving electrophysiological recordings, were perfused using similar methods and solutions, listed below. Once under deep anesthesia, the chest was opened and first saline and then fixative was perfused by peristaltic pump into the cardiovascular system via the heart. Following the fixation, phosphate buffer (PB) was perfused to remove the fixative from the tissue. After fixation the brain was removed from the skull and sectioned using a Leica VT1200s microtome (Leica Biosystems). Slices were cut at 50-60 μm thickness.

Used solutions:

- Saline (0.9% NaCl in H_2O) – 2 minutes
- 4% paraformaldehyde solution in 0.2 M PB (1:2) + 0.1% glutaraldehyde (mixed immediately before perfusion) – 30 minutes, 180 ml
- PB – 50 ml

Preparation of the sections: For cryoprotection, sections were incubated in 30% sucrose overnight or in 10% sucrose for 10 minutes then in 30% sucrose for an hour. Following the sucrose treatment, to unmask antigens in the tissue and help the penetration of the antibodies, sections were frozen over liquid nitrogen 3 times and then washed in tris-buffered saline (TBS) buffer. Alternatively 0.1% triton was used for 30-60 minutes. These sections, however, could not be used for electronmicroscopic (EM) analysis due to the deleterious effect of triton on membrane ultrastructure.

Used solutions:

- 10 and 30% sucrose – 10 minutes, 1 hour and overnight, respectively
- TBS – 3x10 minutes

Immunohistochemistry: For all the reactions TBS buffer was used as a solvent. Following each step, 3x10 minutes rinse with clean TBS was applied. First, the sections were treated with bovine serum albumin (BSA) to mask unspecific antibody binding sites, and then, without washing, primary antibody solution was applied followed by the secondary fluorescent or biotinylated antibody. After washing out the biotinylated antibody, sections were incubated in avidin-biotin horseradish peroxidase complex (ABC), then either in diaminobenzidine (DAB) for brown precipitation or nickel intensified diaminobenzidine (DAB-Ni) for black precipitation. The oxidation of DAB or DAB-Ni was induced by 1% or 0.03% hydrogen peroxide, respectively. In specific cases, ABC was replaced by ImmPRESS (anti mouse/rabbit/goat) peroxidase conjugated secondary antibody, making the procedure faster but less sensitive. Depending on the aim of the experiment various immunoreactions were performed with various antibodies at different concentrations. Details are given in the corresponding paragraph of Materials and Methods.

Used solutions:

- BSA: 3%, 40 minutes
- primary antibodies: sensitivity-dependent concentration, overnight
- secondary antibodies: sensitivity-dependent concentration, 2 hours
- ABC: 1:300-500, 90 minutes
- Immpress: 1:2-1:3, 90 minutes
- DAB/DAB-Ni incubation: 10 minutes
- H_2O_2: 0.03%-1%

Dehydration and embedding of the tissue: to prepare tissue for embedding, sections were treated with OsO_4 (1% for 40 min) followed by sequential incubation in ethanol (50%, 70%, 90%, absolute) and acetonitrile as a final step at room temperature. Between the 70% and 90% ethanol step, uranile acetate solution was applied for 20 minutes. After the dehydration procedure, sections were incubated in Durcupan (ACM, Fluka, Buchs, Switzerland) overnight, followed by curing in fresh durcupan at 60^{o}C for 24 hours.

Used solutions:

- 1% OsO_4 solution (1:2:1 - OsO_4:0.2M PB:H_2O), 20-40 minutes
- ethanol (50%, 70%, 90%, absolute), 10-10 minutes
- uranilacetate (1:10) in 70% ethanol, 20 minutes
- acetonitrile, 2x5 minutes
- Durcupan, overnight

Preparation for electron microscopy: to prepare electron microscopic sections, one region of interest (ROI) was re-embedded from the light microscopic material. The ROI was further sectioned to 60 nm ultrathin sections using an ultramicrotome (EM UC6, Leica Biosystems). Sections were mounted on copper and nickel pioloform-coated grids. In some cases, a post-embedding GABA reaction was performed on sections mounted on nickel grids according to the protocol of Somogyi *et al*. (Somogyi et al., 1985).

3.4.3 Retrograde tracing and immunohistochemistry

PRF-to-IL projection: In order to identify thalamus-projecting brainstem neurons, we injected FluoroGold (FG) iontophoretically (0.6 μA; 2 s on/off period; 10 min duration, capillary tip diameter 20 μm) into the intralaminar thalamus of GlyT2::eGFP mice (n = 6 unilaterally and n = 2 bilaterally). The following co-ordinates were used: Bregma -1.2 mm to -1.7 mm; lateral 0.7 to 0.8 mm, ventral from cortical surface -3.0 to -3.5 mm. After 3 days, mice were anaesthetized and were perfused through the heart. For the fixation, the 0.1% glutaraldehyde and 4% paraformaldehyde containing solution was used. The coronal sectioning of the thalamus and the brainstem (50-60 μm slices) was followed by cryoprotection in 30% sucrose solution overnight. The sections were frozen above liquid nitrogen to unmask the antigens in the tissue.

To detect FG, an anti-FG primary antibody (Chemicon, AB 153, 1:10,000 to 1:30,000, overnight) was used. For light microscopic visualization we applied either a 1 nm gold particle-conjugated goat anti-rabbit secondary antibody (1:50, Amersham) with silver

intensification (Aurion R-Gent SE LM -silver enhancement kit, 20-22min), or long-spacer biotinylated donkey anti-rabbit secondary antibody (b-SP-DARb, Jackson Immuno Research Laboratories Inc., 711-065-152, 1:500) followed by ABC (1:500 Vector) and DAB-Ni (black reaction product) treatement. For fluorescent microscopy, an Alexa 594 conjugated goat anti-rabbit antibody (1:500, Molecular Probes) was used.

Frontal cortex-to-PRF projection: In a separate set of experiments (n = 4) FG was injected into the PRF (2 μA; 7 s on/off period; 15 min duration) to identify its inputs. We used the following coordinates: Bregma -4.4 mm; lateral -0.8 to -1 mm; ventral from cortical surface -4.2 mm. After 5-7 days of recovery, animals were perfused as described above and the entire brain was sectioned coronally.

3.4.4 Anterograde tracing and immunohistochemistry

PRF-to-IL projection: In order to visualize pontothalamic fibers, a *AAV5.EF1a.DIO.hChR2(H134R)-eYFP.WPRE.hGH(Addgene20298P)* cre dependent virus construct (Penn Vector Core, Philadelphia, PA 19104-3403) was injected into the PRF of GlyT2::cre mice at the following coordinates Anteroposterior, Br -4.3 mm to -4.4 mm; Lateral, 0.8 mm; V, -4.0 mm. After the injection, animals were allowed to recover for two weeks, which was enough time for the neurons to express the viral gene constructs. The virus-injected animals were used in anaesthetized and freely moving experiments (see in Chapter 4.3 and 4.4.) and the fiber distribution was determined *post hoc*. The animals were then perfused according to the protocol described in Chapter 3.4.2.

In order to visualize GlyT2::eGFP fibers with light microscopy, the sections were treated with mouse or chicken anti-eGFP antibody (1:20,000, Molecular Probes, A11120, overnight) followed by biotinylated horse anti-mouse or horse anti-chicken secondary antibody (1:300, Vector, 2 hours) respectively, then the sections were treated by ABC (1:300 Vector) and DAB-Ni. In order to label the postsynaptic targets of GlyT2::eGFP fibers in the IL, the eGFP-DAB-Ni immunoreaction was followed by a treatment with a rabbit anti-calbindin antibody (1:20,000, Swant, overnight) and rabbit ImmPRESS (1:2, Vector, 90 min). The calbindin immunostaining was visualized by DAB alone, yielding a brown reaction product.

In order to verify the specificity of the GlyT2::eGFP mouse line, coronal sections of the thalamus from GlyT2::eGFP mice were treated with a guinea pig anti-GlyT2 antibody (1:10,000, Chemicon, AB 1773, overnight) followed by a Cy3 conjugated donkey anti-guinea pig antibody (1:500, Jackson, 2 hours). All GlyT2-positive terminals examined (n = 106) displayed eGFP signal, whereas 95% of the eGFP terminals (n = 311) were immunopositive for GlyT2 (n = 2 animals).

Glycinergic fiber distribution mapping: After showing that the glycinergic innervation originates in the PRF, we mapped the glycinergic fiber distribution in the thalamus. Anti eGFP staining on GlyT2::eGFP or on virus-injected GlyT2::cre mouse sections was performed as described above. Thalamic neurons were visualized using an anti-calbindin-DAB reaction (1:20,000, Swant, overnight).

To compare the distribution pattern of GlyT2 fibers in mice and humans we performed anti GlyT2 immunostaining on human samples. Slices were treated with an anti-GlyT2 antibody (1:10,000, Chemicon) overnight and the signal was visualized with an ABC – DAB-Ni reaction. Postsynaptic targets were labeled with anti-calbindin (1:20,000, Swant, overnight) and visualized with DAB.

The DAB and DAB-Ni reactions were viewed with either a Zeiss Axionplan 2 fluorescent microscope and photographed by a digital camera (Olympus DP70), or with a Zeiss Axio Imager M1 microscope coupled to an AxioCam HrC digital camera. Fluorescent micrographs were taken with an Olympus DP70 digital camera. For confocal images, an Olympus Fluoview FV1000 confocal laser scanning system on an Olympus BX61 microcope, or a Nikon A1R confocal microscope was used.

Primary sensory cortex (S1)-to-POm projection – relative distribution of cortical and subcortical drivers: To examine the projection pattern of S1 cortex and the relative distribution of cortical and subcortical terminals in the POm, anterograde tracing was combined with vGluT2 immunostaining in both rats and mice. Phaseolus vulgaris leucoagglutinin (PHAL, Vector Laboratories) or biotinylated dextran amine (BDA) was iontophoretically injected to the S1 cortex (rats: Bregma −1.2 mm, lateral −5.0, ventral from cortical surface: 1.5mm, mice: Bregma −1.2 mm, lateral −3.0, ventral from cortical surface:

0.8 mm) using the following parameters: PHAL: 2.5% in 0.01 M PB, 5 μA, 7 s on/off duty cycle, 20 min; n = 5 mice and n = 6 rats, BDA: 2 μA, 2 s on/off, 20 min, pipette d = 15 μm, n = 4 rats. After a survival period of 5–7 days, mice were perfused according to the standard procedure described in Chapter 3.4.2 (4% paraformaldehyde solution + 0.1% glutaraldehyde). Rats were perfused with a 2-component fixative: first component: 2% paraformaldehyde 0.1–1% glutaraldehyde in acetate buffer (100 ml), second component: 2% PF 0.1–1% glutaraldehyde in borate buffer (400 ml). The subsequent sectioning and preparation procedures were carried out as described in Chapter 3.4.2.

Anterogradely-labeled axon terminals in the POm were reacted with a rabbit-anti-PHAL antiserum (1:10,000) and biotinylated anti-rabbit IgG (1:500, Jackson) and visualized with DAB-Ni (see Chapter 3.4.2). BDA was developed with avidin biotinylated horseradish peroxidase complex and visualized with DAB-Ni. To visualize vGluT2 terminals, an anti-vGluT2 antibody was used (1:3000, Chemicon) followed by mouse ImmPRESS (1:3, Vector, 3 h) and a DAB reaction (see: Chapter 3.4.2).

To quantify the co-distribution of the cortical (labeled by PHAL) and subcortical (vGluT2) terminals, we calculated the portion of large cortical terminals (n = 1027 terminals, 3 animals) within zones of POm "rich" or "poor" in vGluT2-positive terminals (n = 3 animals). We defined vGluT2-rich zones as counting more than 15 terminals in a 100 × 100 μm area on the top and bottom surface of the section using a 63× oil immersion objective (1.4 numerical aperture). Photomicrographs were acquired with an AxioCam HRC (Carl Zeiss Microimaging, Jena, Germany) camera. Photomicrographs were processed by Image-Pro Express 6.0 (Media Cybernetics, Bethesda, MD, USA, "extended depth of field function") and Adobe Photoshop CS2 (Adobe Systems, San Jose, CA, USA). Modifications were applied to whole images only.

Frontal cortex-to-PRF projection: To examine the motor cortex projection to the PRF, we injected a *AAV5.EF1.dflox.hChR2(H134R)-mCherry.WPRE.hGH (Addgene20297)* cre dependent virus into the cortex of GlyT2::eGFP/Rbp4::cre mice. Layer 5 pyramidal neurons were transfected and after 2 weeks their fiber distribution in the brainstem was analyzed. To visualize the virus-infected fibers, an anti-mCherry primary antibody (BioVision, Inc.,

California 95035, 1:4000) was used, followed by either anti-rabbit ImmPRESS (1:2, Vector Laboratories Burlingame, Ca 94010) and DAB-Ni as a chromogen for light microscopic analysis, or a Cy3-conjugated goat anti rabbit secondary antibody for fluorescent microscopic analysis.

In previous experiments, PHAL was injected in the frontal motor cortex area to label PRF-projecting fibers. To visualize the axons, an anti-PHAL primary antiserum (Vector Laboratories Burlingame, Ca 94010, 1:30000) was used, followed by a biotinylated goat anti-rabbit secondary antibody (1:300, Vector Laboratories Burlingame, Ca 94010) and ABC (1:300, Vector Laboratories Burlingame, Ca 94010) treatment, and finally DAB-Ni as a chromogen. For fluorescent microscopy, PHAL was visualized by a rabbit anti-PHAL (1:10,000, Vector Laboratories Burlingame, Ca 94010) primary antibody and an Alexa 594-conjugated goat anti-rabbit secondary antibody.

3.4.5 Electron microscopy

Ultrastructural analysis of PRF axons: The ultrastructure of PRF axons in the IL were examined using ultrathin electron-microscopic sections (60 nm). To prepare for electron-microscopic analysis, mice were perfused with sequentially applied 2-component fixative: first component: 2% PF 0.1–1% glutaraldehyde in acetate buffer (100 ml), second component: 2% PF 0.1–1% glutaraldehyde in borate buffer (200 ml). To visualize eGFP, a silver-intensified pre-embedding immunogold reaction was used (mouse anti-eGFP 1:1000 followed by a 1nm gold particle-conjugated goat anti-mouse secondary antibody). Following the immunoreaction, sections were treated with OsO_4 (0.5% for 20 min. at 4 ºC in 0.1 M PB) and were then embedded and prepared for electron-microscopic analysis (for details see: 3.4.2). To visualize GABA, a post-embedding GABA immunostaining was performed on sections collected on nickel grids (see: 3.4.2). Electron micrographs were taken using a Megaview digital camera installed in a HITACHI 7100 electron microscope. For 2D measurements, ITEM software (Olympus Soft Imaging System) was used.

Target diameter mesurements of cortical and subcortical drivers: to determine the targeted dendritic domain of labeled cortical and subcortical terminals at the electron microscopic

level, the minor dendritic diameter of a random sample or a given target dendrite was measured. The dendritic diameter was the average of 3 diameters measured on non-consecutive electron-microscopic sections with synaptic contacts. As the data did not have normal distribution, statistical significance of the difference of dendritic domains targeted by driver terminals and random dendritic regions was assessed by using the non parametric Mann–Whitney U test.

3.4.6 Human tissues preparation

Re-embedding and electron-microscopic studies were performed as described in Chapter 3.4.2. Human tissues were previously prepared for light microscopic analysis. The methodological description is qoted from Giber, Diana, Plattner and colleagues (Giber et al., 2015):

Brains were removed 4-5 hours after death. The internal carotid and the vertebral arteries were cannulated, and the brains were perfused first with physiological saline (1.5 L in 30 min) containing heparin (5 ml), followed by a fixative solution containing 4% paraformaldehyde, 0.05% glutaraldehyde and 0.2% picric acid in 0.1 M PB, pH=7.4 (4-5 L in 1.5-2 hours). The thalamus was removed from the brains after perfusion, and was postfixed overnight in the same fixative solution, except for glutaraldehyde, which was excluded. Subsequently, 50 μm thick coronal sections were obtained for immunohistochemistry using a Leica VTS-1000 Vibratome (Leica Microsystems, Wetzlar, Germany). The sections were incubated with a guinea pig anti-GlyT2 antibody (1:10,000, Chemicon), and the signal was visualized with the DAB-Ni reaction described above. The sections were then treated with OsO_4 (1.0% for 40 min. in 4 °C in 0.1M PB), dehydrated in ethanol and acetonitrile, and embedded in Durcupan (ACM, Fluka, Buchs Switzerland). Ultrathin sections were cut with an Ultramicrotome from blocks containing GlyT2-positive fibers. In some cases postsynaptic IL neurons were visualized using a mouse anti-calbindin antiserum and DAB reaction. In these cases, glucose (7%) was added to the OsO_4 solution to preserve the color difference.

3.5 In vivo physiology

3.5.1 Surgery

Altogether 20 adult male C57Bl/6J BAC GlyT2::eGFP and GlyT2::cre mice (20-30g) were used for the experiments. Surgery, acute recording experiments and implantations were done under ketamine/xylazine anaesthesia. The head of the animal was fixed in a stereotaxic apparatus (David Kopf Instruments, Tujunga, California 91042, Model 900 Small Animal Stereotaxic Instrument). Initially, mice received an intraperitoneal injection of ketamine (111 mg/kg) and xylazine (4.3 mg/kg). For the maintenance of the anaesthesia, intramuscular injection of ketamine/xylazine was given every 30-50 min during the experiments.

3.5.2 In vivo juxtacellular recording and labeling, local field potential (LFP) recording

Bipolar LFP electrodes (FHC, resistance ~1 MΩ) were inserted into the frontal cortex of mice (Bregma 1.7 mm; lateral -0.8 mm). The recorded signal was amplified, band-pass filtered from 0.16 Hz to 5 kHz and from 100 Hz to 5 kHz to record the fast multiunit activity (Supertech BioAmp, Supertech, Pécs, Hungary) and digitized at 20 kHz (micro 1401 mkii, CED, Cambridge, UK). Concentric bipolar stimulating electrodes were inserted into the IL (Bregma -1.5 mm; lateral 2 mm; ventral from cortical surface -3.2 mm tilted at 20 degrees, electrode separation 0.8mm). PRF single unit activity was recorded by glass microelectrodes (*in vivo* impedance of 20-40 MΩ) pulled from borosilicate glass capillaries (1.5 mm outer diameter, 0.75 or 0.86 inner diameter, Sutter Instrument Co., Novato, CA, USA or WPI Inc. Sarasota, Fl, USA) and filled with 0.5 M K^+- acetate and 2% neurobiotin (Vector Laboratories, Burlingame, CA, USA). Electrodes were lowered by a piezoelectric microdrive (Burleigh 6000 ULN or ISS 8200, EXFO, Quebec City, Quebec, Canada) into the PRF (Bregma -4.4 mm; lateral -0.8 to -1 mm; ventral from cortical surface -3.8 to -4.8 mm). Neuronal signals were amplified by a DC amplifier (Axoclamp 2B, Axon Instruments/Molecular Devices, Sunnyvale, CA, USA), further amplified and filtered between 0.16 Hz and 5 kHz by a signal conditioner (LinearAmp, Supertech). Neuronal

signals were recorded by Spike2 5.0 (CED). Juxtacellular labeling of the recorded neurons was done as described previously (Pinault, 1996). Briefly, after recording the activity of the cell positive current steps (0.5-8 nA) were applied at 2 Hz via the recording pipette filled with neurobiotin. The neuron fired only during these current steps. During the induced firing neurobiotin was taken up by the cell filling the soma and proximal dendrites. In some cases, distal dendritic regions and axons were also labeled.

Following perfusion, coronal sections (50 μm) were cut from the PRF and the neurons were visualized with Cy3 conjugated streptavidin (1:2,000, Jackson). GlyT2::eGFP positivity was determined by confocal microscopy. The neurons were then developed using ABC and DAB-Ni, and the sections containing the labeled neurons were dehydrated and embedded in Durcupan. The dendritic trees of the labeled neurons were reconstructed using Neurolucida 5.2 software (MBF Bioscience, Magdeburg, Germany).

3.5.3 Analysis

To find the action potential clusters of the PRF cells, we used a built-in script of the Spike2 7.0 (CED) software. We determined clusters by separating the two peaks at the minimum of the bimodal inter-spike interval histograms (ISI). To determine the phase of each action potential relative to the cortical population activity, we used a previously described method (Slézia et al., 2011). Briefly, the envelope of the cortical multiunit trace (MUA envelope) was low-pass filtered at 4 Hz using a zero phase-shift finite impulse response filter. We calculated the Hilbert-transform of the filtered- and z-scored MUA envelope, and the phase was determined by taking the angle of the complex 'analytic signal'. The prime advantage of this method is that it estimates the phase of any quasi-rhythmic signal (cortical slow oscillation under ketamine-xylazine anesthesia) in a temporally refined manner, defining a time series that quantifies the "instantaneous phase" of the ongoing oscillation. The circular mean angle was calculated for each recorded neuron, and the inter-quartile range was determined as the ±25th percentile around the circular mean.

3.5.4 In-vivo optogenetics and LFP recordings

Two weeks after transfection of PRF cells with an *AAV2-EF1a_DIO-hChR2(H134R)-EYFP* virus (for control experiments: *AAV2-EF1a DIO-EYFP WPRE hGH*) GlyT2::cre animals were anaesthetized with ketamine-xylazine (111 and 5 mg/kg) and placed in a stereotaxic frame. The skin was removed over the frontal, parietal and occipital hemispheres and the skull was cleaned with H_2O_2. All together either six or seven craniotomies were performed; five for the screw electrodes (two over frontal, two over parietal cortical areas and one over the cerebellum for reference and grounding); one or two for the optic fibers (Thorlabs, FG105UCA, Ø105 μm core, 0,22 NA) over the central lateral thalamic and parafascicular nucleus (Bregma -1.9 to 2.3 mm; lateral -0.8 mm; ventral from cortical surface -2.5 to -2.8 mm). The implant was wrapped in copper grid and fixed with Paladur dental cement. The animal was allowed to recover on a heating pad. Mice were rested in their home cage for at least 5 days before testing.

We used the following custom optical system for fiber optic light delivery in freely moving mice: the beam was generated by a 473 nm DPSS laser (LRS-0473-PFM-00050-03, Laserglow Technologies, Toronto, Canada) and was directed to a fiber optic patchcord (Thorlabs) via a fiber port (Thorlabs). The patchcord (1.6 m) was connected to the mouse and allowed to rotate passively. With adequate beam alignment, rotations induced power fluctuations of less than 5% at the fiber output. The power density measured at the output of the delivery fiber was 318 mW/mm^2 for the 200 μm-diameter optic fiber (behavioral experiments) and 1272.73 mW/mm^2 for the 100 μm-diameter fiber (electrophysiological experiments).

To monitor brain activity in freely moving animals, we either used bipolar local field potential (LFP) recording electrodes implanted into the frontal cortex, or in a different set of experiments screw electrodes placed above the same cortical area. A screw electrode served as the ground and reference, and was placed over the cerebellum. Both the recording electrodes and the reference electrode were soldered to a 18 Position Dual Row Male Nano-Miniature Connector (A79014-001, Omnetics Connector Corporation, 7260 Commerce

Circle East, Minneapolis, MN - 55432). For LFP measurements, 30 second-long stimulations were used (3-5 stimulations per day with 5-10 minutes between them). To record the LFP signals we used a 128 channel amplifier (Amplipex Ltd., Hungary). For wavelet generation, we used homemade MatLab scripts.

Behavioral analysis was performed in Paris by our collaborator Marco M Diana on video recordings of motility experiments independently performed both in Budapest and Paris. The methodological description is quoted from Giber, Diana, Plattner and colleagues (Giber et al., 2015):

"For motility tests each mouse was tested in 6 sessions, with a maximum of one session per day. During each session, mice were allowed to move freely on an open white platform, while being filmed continuously via a CCD camera (Guppy Pro, Allied Vision Technologies, Stadtroda, Germany) and exposed to 10 s trains of 5 ms light pulses delivered at 30 Hz every minute for 15 min. Photostimulation trains were signaled on the video recording by an infrared LED. All aspects of the experiment (photostimulation waveform generation, MDS and LED control, video recording) were controlled using LabVIEW (National Instruments Corporation, Austin, TX). Movies were analyzed off-line with Ethovision (Noldus Technology, Wageningen, Netherlands) in order to extract animal trajectories and speed profiles. Statistical comparisons were performed using the Mann-Whitney U test or the Wilcoxon signed rank test for paired sets of data.

Statistics

Statistical comparisons were performed using the Mann-Whitney U test, the Wilcoxon signed rank test for paired sets of data and in the case of the data of Figure 3I-J, a paired t test. Statistical significance was set at $p < 0.05$ but the exact values are reported. Results are given as mean ± SEM. No statistical methods were used to predetermine sample sizes but our sample sizes are similar to those reported in previous publications (21, 27, 35). Equal variances were not formally tested. For more details, see the NN reporting checklist. For the behavior experiments mice were randomly assigned to hChR2.eYFP and eYFP groups. For anatomical, in vitro and in vivo physiological experiments no exclusion criteria was applied for the initial selection and data were collected randomly. All physiology data were

processed by automated software, eliminating the possibility of biases in data processing. The experimenters were not blind to the conditions of the animals. A supplementary methods checklist is available."

4 Results

Part I – Novel source of inhibition in the thalamus

4.1 Distribution of glycinergic fibers in the thalamus, retrograde tracing, origin of the pathway

Besides the well known inhibitory input from the GABAergic neurons of the TRN, particular thalamic nuclei recive inhibition from several other sources (Bartho et al., 2002; Bokor et al., 2005; Bodor et al., 2008). These so-called extrathalamic inhibitory inputs, as well as the TRN input, are purely GABAergic. In a GlyT2::eGFP transgenic mouse line, however, we discovered a massive glycinergic inhibitory input innervating the IL thalamic nuclei (Fig. 4.1.1 a-b) (Giber et al., 2015).

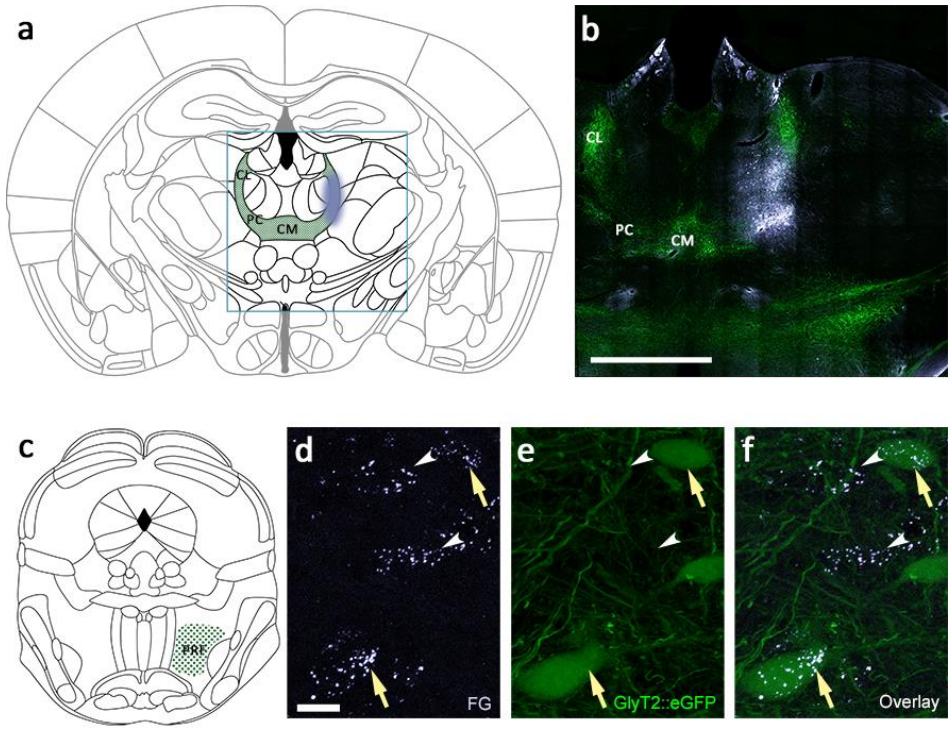

Figure 4.1.1. Retrograde labeling from the IL.

a) Schematic view of the intralaminar thalamic nuclei (green) and the location of fluorogold injection (blue). **b)** Fluorescent micrograph of the glycinergic fibers and the fluorogold injection in the IL thalamus. **c)** Schematic view of the nucleus pontis oralis in the brainstem reticular formation. **d-f)** Retrogradely backlabeled glycinergic (arrow) and nonglycinergic (arrowheads) neurons from the IL in the PRF.

To identify the IL-projecting glycinergic neurons, we injected FG as a retrograde tracer among the glycinergic fibers in the thalamus to different antero-posterior coordinates (Fig. 4.1.1 a-b). The injection site was restricted to the CL (Bregma -1.2, -1.4 mm; lateral 0.8 mm; ventral from cortical surface 3 mm) and Pf (Bregma -2.0, 2.3 mm; lateral 0.8, 0.9 mm; ventral from cortical surface 3.4 mm) of the IL complex. We observed fluorogold-positive backlabeled neurons in the ipsilateral pontine reticular formation (PRF), consisting of the oral and caudal part of the pontine reticular nucleus (PnO and PnC respectively). 55.3% of the thalamus-projecting cells expressed glycine, while the rest were glycine negative (n = 765 cells in 6 animals; Fig. 4.1.1 c-f).

In order to confirm the existence of the pathway and to map the projection pattern of the glycinergic neurons in the forebrain, we anterogradely labeled the glycinergic fibers by injecting a cre-dependent virus construct (see Chapter 3.4.4) into the PRF of GlyT2::cre transgenic mice. Before further analysis, we validated the selectivity of cre expression in glycinergic neurons by crossing the GlyT2::cre and the GlyT2::eGFP lines and performing anti-cre immunostaining. We found that out of 198 cre-positive cells, 196 (99%) were also eGFP positive (Fig. 4.1.2 a-c). After the virus injection, we observed similar fiber distribution patterns in the thalmus as we did in the GlyT2::eGFP transgenic mice (Fig 4.1.3).

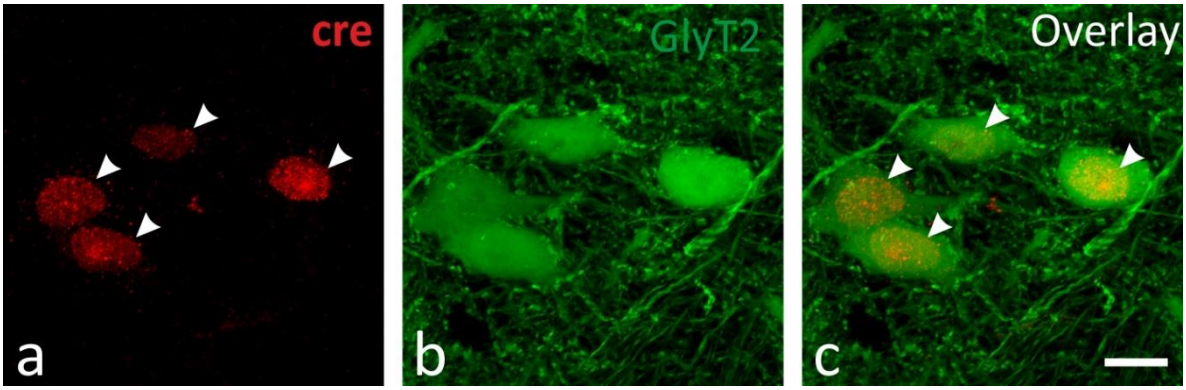

Figure 4.1.2. Validation of selective cre expression in the glycinergic neurons.

a) Nuclei of glycinergic cells visualized by cre immunostaining. **b)** Glycinergic neurons in the PRF. **c)** Overlay.

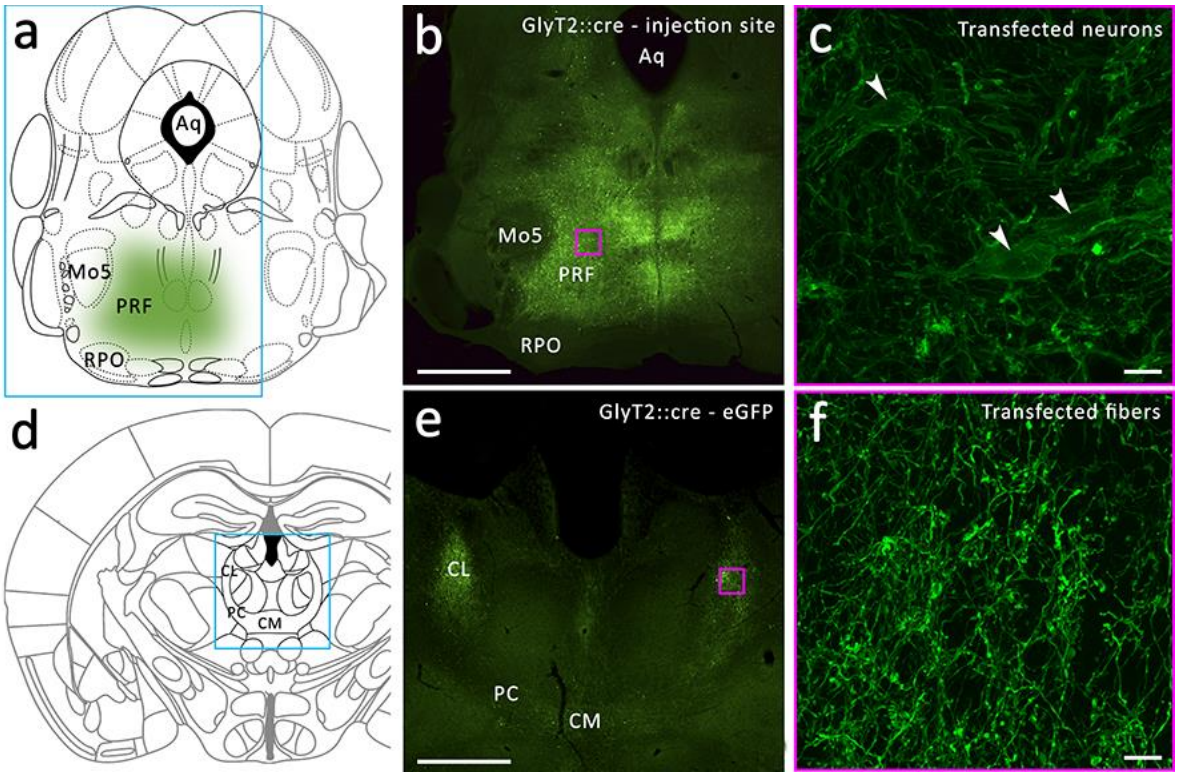

Figure 4.1.3. Anterograde virus tracing from the PRF in GlyT2::cre animals.

a) Schematic view of the injection site in the PRF. **b)** Fluorescent micrograph of the injection site in the PRF. **c)** Higher magnification of the transfected glycinergic cells. **d)** Schematic view of the distribution of the glycinergic fibers in the IL after anterograde labeling. **e)** Fluorescent micrograph of the transfected glycinergic fibers in the IL. **f)** High magnification fluorescent micrograph of the glycinergic fibers in the IL.

To visualize the innervated thalamic relay cells and to identify the targeted dendritic domain, we used calbindin (CB) – eGFP double immunostaining. We found that the glycinergic neurons targeted the soma and proximal dendritic regions of thalamic neurons (Fig. 4.1.4 b, d). Electron-microscopic analysis and postembedding GABA staining (Somogyi et al., 1985) revealed that the fibers ended in large terminals (5-8 μm), coreleased GABA and glycine, and contacted the relay cells via multiple synaptic release sites (2-14). These pre- and postsynaptic structural properties made possible the extremely effective and faithful non-depressing connection between the PRF glycinergic-GABAergic neurons and their thalamic target neurons.

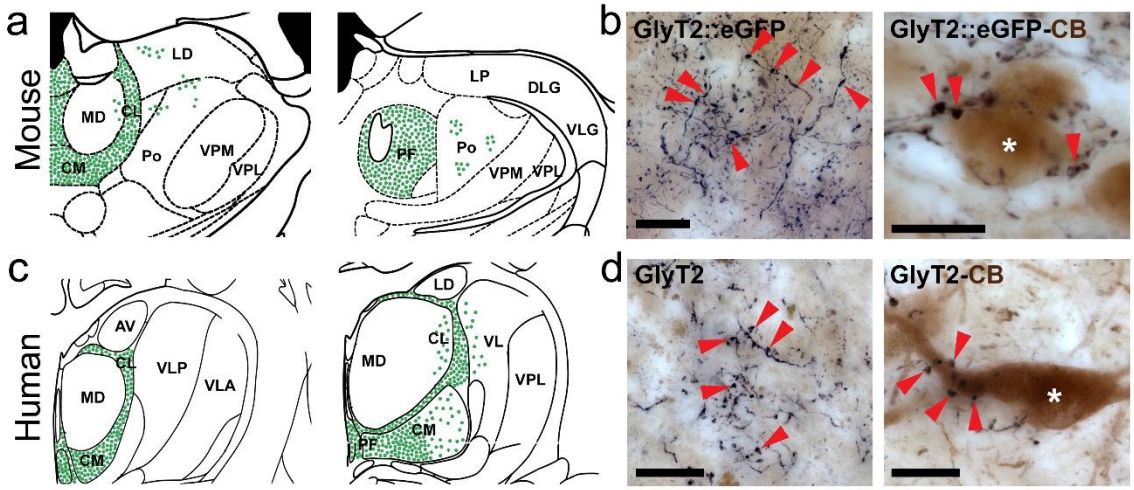

Figure 4.1.4. Distribution of glycinergic fibers in mouse and human.

a) Schematic view of the distribution of glycinergic fibers in the mouse thalamus. **b)** Glycinergic fibers visualized by DAB-Ni (left) and glycinergic fibers targeting the soma and proximal dendrites of CB positive (visualized by DAB) thalamic cells (right). **c)** Schematic view of the distribution of glycinergic fibers in the human thalamus. **d)** Same as in (**b**) shown in human. Scale bars: 20 μm.

The importance and evolutionarily-conserved nature of the pathway is supported by the finding that similar glycinergic innervation of the IL is also present in humans (Fig. 4.1.4 c-d). We used GlyT2 – CB double immunostaining to visualize the glycinergic fibers and the thalamic relay cells, respectively, in human tissue samples (n = 3). The comparison with rodent data showed that the glycinergic fibers distributed homologously within the human thalamus (Fig. 4.1.4 c-d) and had similar morphological properties at the ultrastructural level in both species (Fig. 4.1.5).

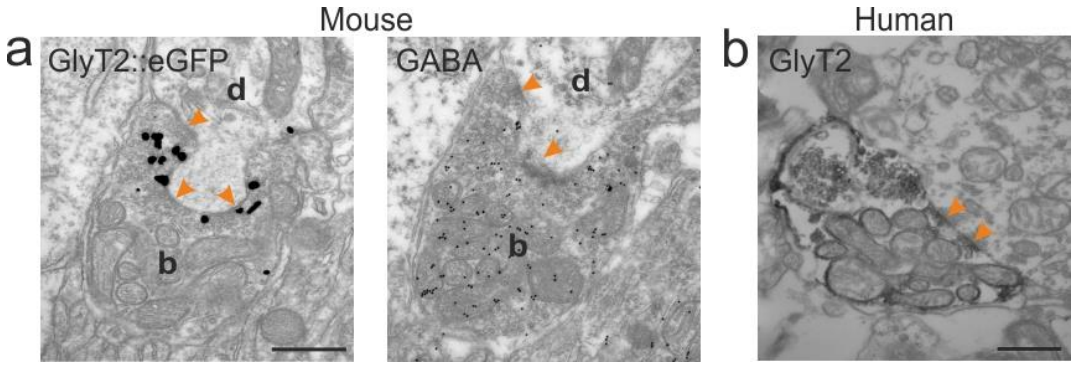

Figure 4.1.5. Electronmicrographs of glycinergic terminals in mouse and human.

a) On the left, a preembedding immunogold reaction against eGFP labels a glycinergic terminal (large black dots). On the right postembedding GABA reaction was performed on the neighbouring serial section of the same terminal, indicating its GABAergic phenotype. **b)** A glycinergic terminal labeled by DAB-Ni in a human sample. Note that glycinergic terminals have multiple release sites in both species (arrowheads). Scale bars: 500nm.

In summary, the tracing studies in rodents and the immunohistochemistry on human tissues revealed a new source of inhibition in the IL thalamus originating from the brainstem. This pathway co-expresses glycine and GABA, the two main inhibitory neurotransmitters, and forms effective inhibitory connections with thalamic relay cells.

4.2 Activity of glycinergic neurons in anaesthetized animals

To anticipate the putative effects of the glycinergic input in the thalamus, we first need to understand the activity of the glycinergic neurons. To do so we used juxtacellular single unit recording and labeling in the PRF, combined with frontal cortical LFP recordings under ketamine-xylazine anesthesia (n = 11 neurons in 11 animals, Fig. 4.2.1). Although ketamine-xylazine anaesthesia is an artificially generated and maintained state of the nervous system with several altered cellular and network properties compared to natural slow wave sleep (SWS), the main features of the slow oscillations are reproduced (Chauvette et al., 2011). Thus this preparation allowed us to explore – at least in one stabilized state – the activity of the glycinergic cells in the PRF.

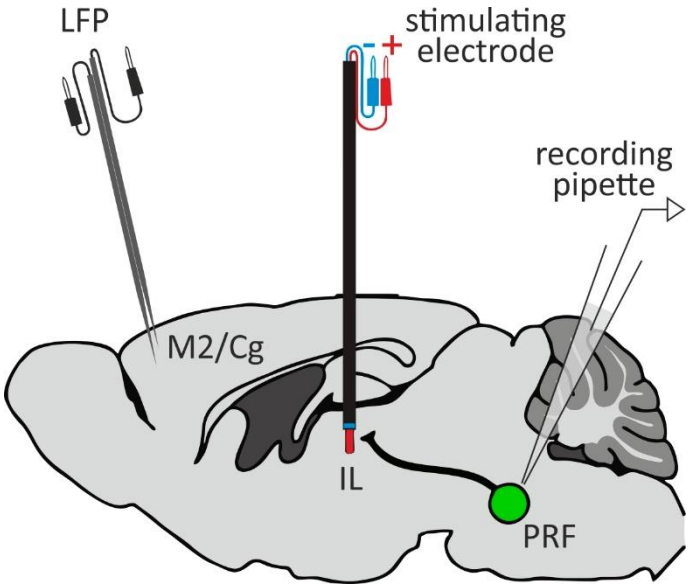

Figure 4.2.1. Electrode arrangement for juxtacellular recording in the PRF

We found that 8 out of 11 recorded and *post hoc* identified GlyT2 positive neurons fired rhythmic clusters of action potentials (AP) interspersed with silent periods (Fig. 4.2.2 a, b), while 3 neurons showed no or very low firing activity. The mean firing rate (MFR) of the neurons as well as the intra-cluster frequency (within and across cells) were quite variable and changed between 2-23 Hz and 12-100 Hz (mean = 41.34 ± 11.59, median = 29Hz) respectively. The firing parameters of each cell are summarized in Table 1.

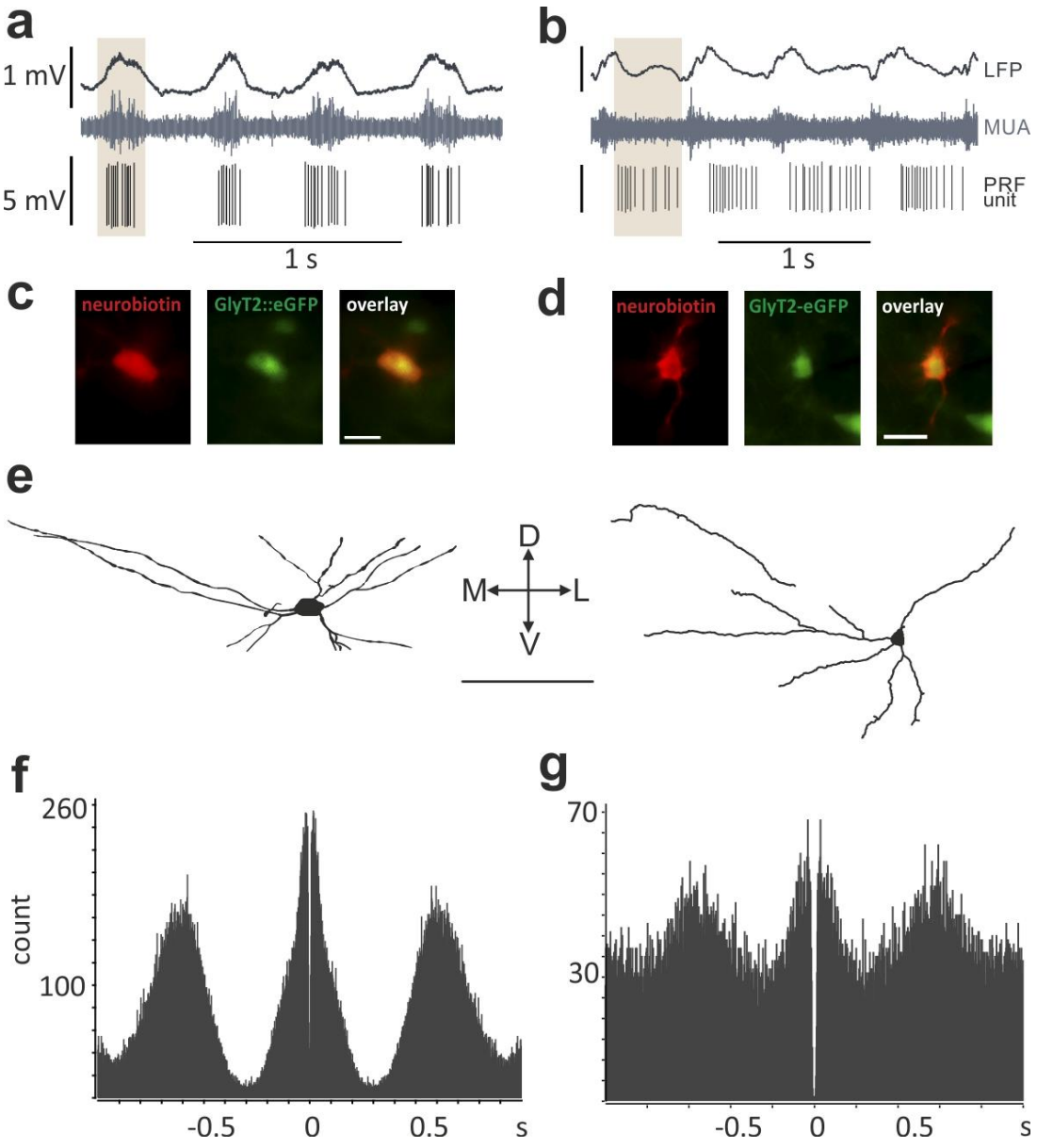

Figure 4.2.2. Baseline activity of the PRF glycinergic neurons.

a-b) Rhythmic clusters of action potentials coupled to the active (**a**) or inactive phases of the cortical slow oscillation (**b**). **c-f)** Individually labeled and reconstructed recorded neurons. **g-h)** Autocorrelograms of the two example neurons. Note the rhythmic firing pattern in both cases.

The recorded AP clusters appeared to be coupled to the cortical slow oscillation. To analyze the phase modulation of the PRF neurons, we calculated the Hilbert transform of the cortical LFP (Phase analysis was performed by Balázs Hangya). The phases of the action potentials

were determined by the angle of the analytic signal at the location of spikes. In our case, the peak of the Up-state represented 0°, and the trough 180°. We found that in the case of each cell, AP clusters occured at particular phases of the cortical oscillation, and together they covered the whole Up-Down cycle (Fig. 4.2.3). To test the uniformicity null hypothesis, Rao's spacing test was performed in each case (Rao, 1976), showing highly significant phase coupling (Table 1.).

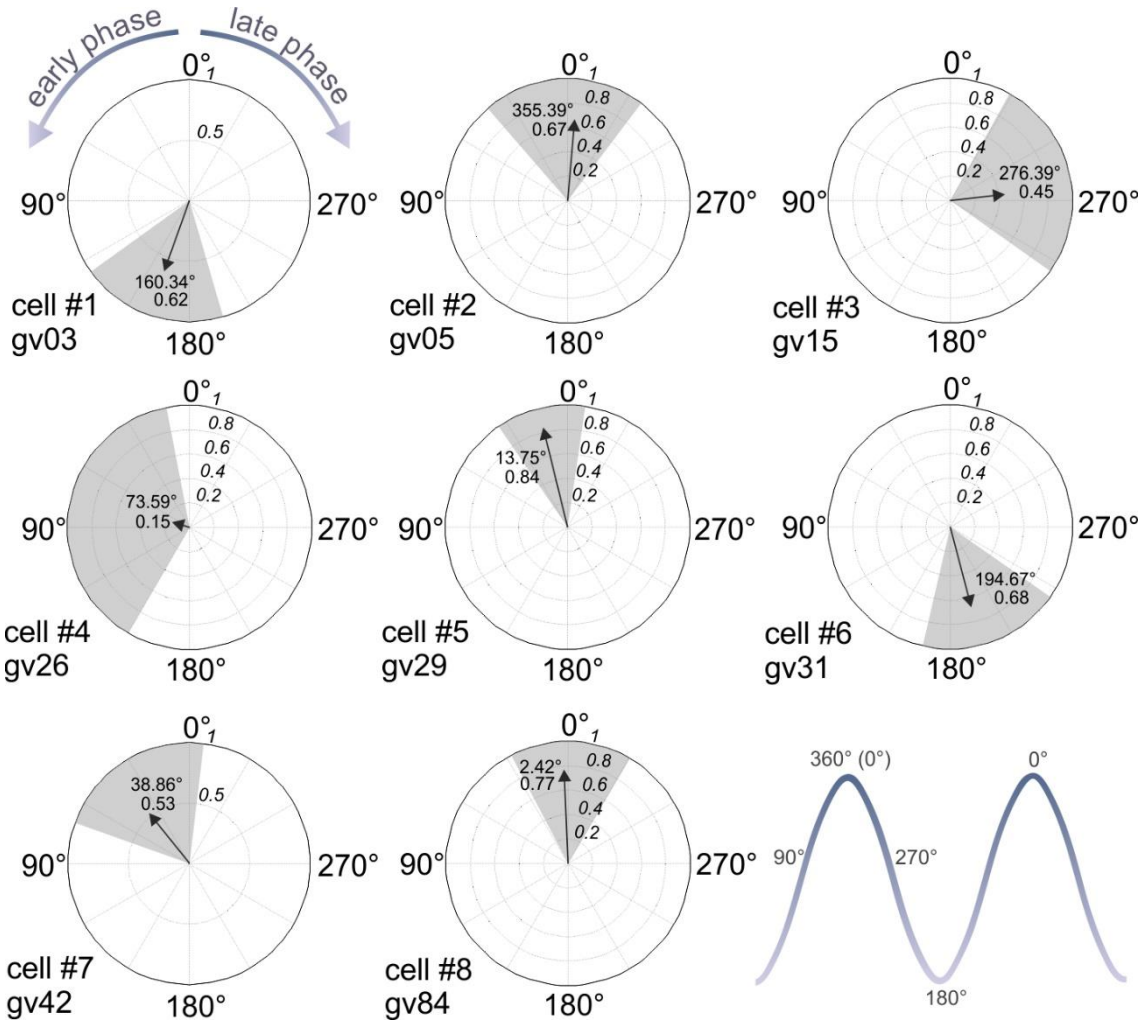

Figure 4.2.3. Phase coupling of eight recorded and identified glycinergic neurons.

Grey sections show the phase preference of the AP clusters. Mean angle is represented by the direction of the vector (black arrow). Its length is proportional to the strength of the phase coupling. A schematic view of two slow oscillation cycles is shown in the lower right panel.

In the two most extreme cases, AP clusters were either strictly coupled to the peak of the active phases of the cortical oscillation or occurred during the inactive phases, as shown in Figure 4.2.2 a, b and Figure 4.2.3 (cell #1 gv03 and cell#2 gv05). These neurons were 3D reconstructed and proved to have large dendritic trees spanning across the PRF in the mediolateral direction (Fig. 4.2.2 e). The autocorrelograms indicated rhythmic phase modulation of the cells (Fig. 4.2.2 f, g).

	firing properties				phase		
cell ident. code	**FR**	**FR during cortical inactivation**	**# spikes/cluster (n = 50)**	**ICFR (n = 50 clusters)**	**mean angle (°)**	**mean resultant length**	**Rao's p value**
GV03_4294	23	na	13.2±4.3	42.84 ± 6.4	160.34	0.62	<0.001
GV05_3940	18	5	11.1±2.7	81.4±31	355.39	0.67	<0.001
GV15_4449	4	6	4.2±2	21.8±11.6	276.39	0.45	<0.001
GV26_4549	2	na	2.4±1	13.8±7.3	73.59	0.15	<0.01
GV29_4245	3	1	4.7±2.4	35.8±21.7	13.75	0.84	<0.001
GV31_4461	6	16	4.3±2	12.1±3.9	194.67	0.68	<0.001
GV40_4153	10	5	7.2±3	100.7±43.1	no MUA envelope		<0.001
GV42_4227	2	0	1 (sometimes doublets)		38.86	0.53	<0.001
GV84_4200	3	na	3.5±1.5	22.2±13.4	2.42	0.77	<0.001

Table 1. Firing and phase coupling properties of nine identified glycinergic neurons. **FR**: firing rate.

To test if the recorded PRF neurons were indeed thalamus-projecting, we electrically stimulated the IL thalamus and recorded the antidromic response of the cell in the same preparation (Fig. 4.2.4). To consider a response to be antidromic, we used two criteria. On the one hand we expected the evoked APs to occur with short (1-2 ms) latency, with almost no jitter, as the axonal conductivity is supposed to be the same across trials, and on the other hand we expected no failures. We could evoke reliable antidromic APs in two cases, while in the rest the responses did not match our criteria. It is important to emphasize that this could

be due to the arrangement and properties of the stimulating electrode. We could only stimulate a small region, and thus a limited number of fibers in the IL, without destroying the tissue, so it is very likely that the recorded neuron in the PRF did not have fibers in close proximity to the electrode.

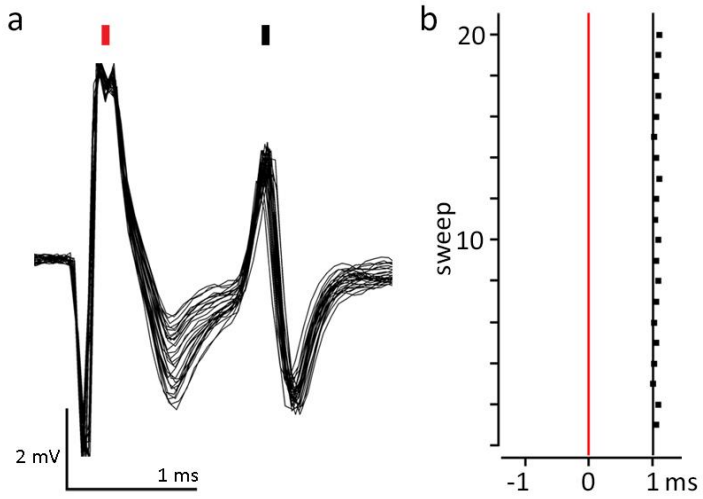

Figure 4.2.4. Antidromic activation of a recorded PRF neuron from the thalamus.

a) Superposition of APs aligned to the stimulus (red tick, stimulus artefact; black tick, evoked APs). **b)** Rasterplot of the antidromically-evoked APs aligned to the stimulus (red line). Note the short latency and small jitter of the evoked APs.

In these experiments we have shown that the glycinergic neurons in the PRF fired rhythmic clusters of APs. The clusters were coupled to particular phases of the cortical slow oscillation and showed strong phase modulation.

4.3 Activation of the pathway, effects on thalamic neurons

To investigate the effect of the glycinergic pathway on the firing properties of thalamic neurons, and thus on TC activity, we recorded single units in the IL combined with LFP recordings in the frontal cortex (n = 2). In these experiments we used urethane anaesthesia because, in contrast to ketamine-xylazine, urethane does not have a powerful synchronizing and stabilizing effect on thalamocortical activity and on thalamic firing (Chauvette et al., 2011). Instead, intermingled cortical oscillations with different dominant spectral

components can be observed that makes it easier to interact with the system; i.e. disrupt or synchronize its activity and examine the induced changes.

The experiments were performed in GlyT2::cre transgenic animals after selective transfection of the glycinergic neurons using the cre-dependent virus construct (see Chapter 3.4.4). This transfection allowed us to selectively photoactivate glycinergic fibers around the recorded IL neurons. We set the stimulation parameters according to the previously recorded firing properties of the glycinergic neurons in the brainstem. As rhythmic AP clusters of the glycinergic neurons did not occur at the same phase of the cortical oscillation, but covered the whole Up-Down cycle, we assumed that IL thalamic neurons receive a tonic and continuous inhibition from the PRF at the population level (Fig. 4.2.3). The intracluster frequencies within and across neurons were quite variable (described above), lacking a single representative value, so for the photoactivation of the glycinergic fibers we chose to use the median value (~30Hz) of the intracluster firing frequency of the glycinergic cells instead of the average. Using this we could capture the tonic and continuous aspect of the inhibition: however, the role of the variability in firing rate remained unclear.

The baseline activity of the recorded thalamic neurons was not uniform. They either showed tonic-like activity with a high (25 Hz) baseline firing rate and with higher frequency clusters of APs during cortical Up-states (Fig. 4.3.1 a), or their baseline firing was low (8 Hz) and high frequency (15 Hz) tonic firing could be induced by tail pinch (Fig. 4.3.2 a).

In the former (tonic-like firing) case, we applied 30 Hz light stimulation to the glycinergic fibers for 30 seconds and found that thalamic firing was completely inhibited during the inactive periods of the cortical oscillation, and only the high frequency clusters remained (Fig. 4.3.1 a). Consequently, a second peak appeared on the previously unimodal inter-spike interval histogram, indicating the clustered firing activity of the cell (Fig. 4.3.1 b, c), and the STAs became modulated (Fig. 4.3.1 d, e). After the light stimulus offset, the tonic-like firing immediately returned.

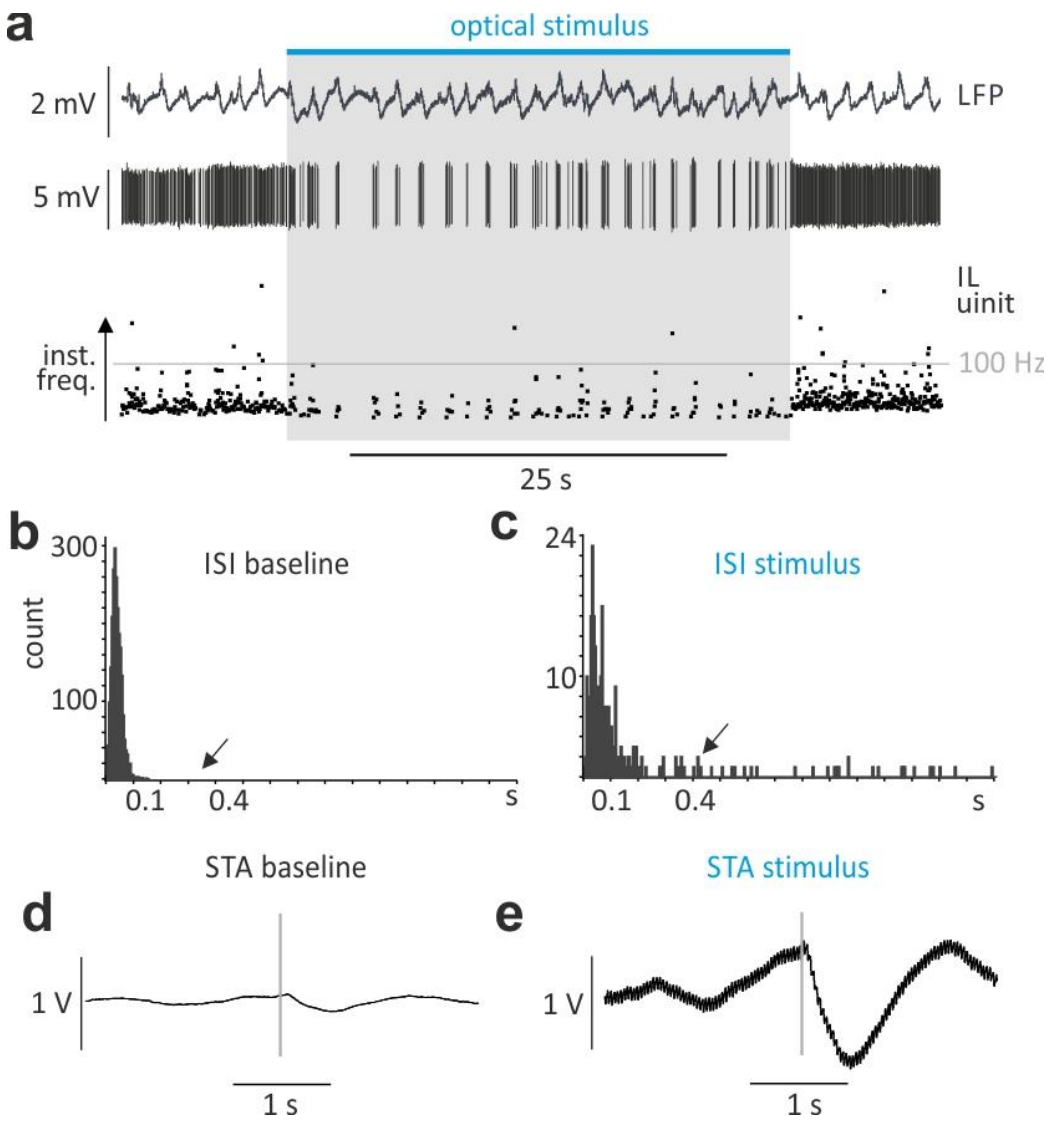

Figure 4.3.1. Photostimulation-induced glycinergic inhibition of a tonically active IL thalamic neuron.

a) Firing pattern of a recorded IL thalamic neuron before, during and after the photoactivation of the surrounding glycinergic fibers. Note the increased firing frequency during the cortical active periods. **b-c)** Inter-spike interval histograms before and during stimulation. Note the second smaller peak in the case of stimulation, indicating the increased inter-cluster intervals. **d-e)** Spike triggered averages before and during stimulation. Note the stimulus-induced increase in modulation on panel (**e**).

In the latter (tail pinch) case, we could observe the effect of glycinergic inhibition not only on a single IL thalamic neuron but also on thalamocortical activity. Since tail pinch is a painful stimulus, it also serves as a waking signal, and under urethane anesthesia this could

on the one hand increase IL firing, and on the other hand desynchronize thalamocortical oscillations (Fig. 4.3.2 a). Under this condition we monitored the effect of consecutive activation of the glycinergic pathway on thalamocortical activity.

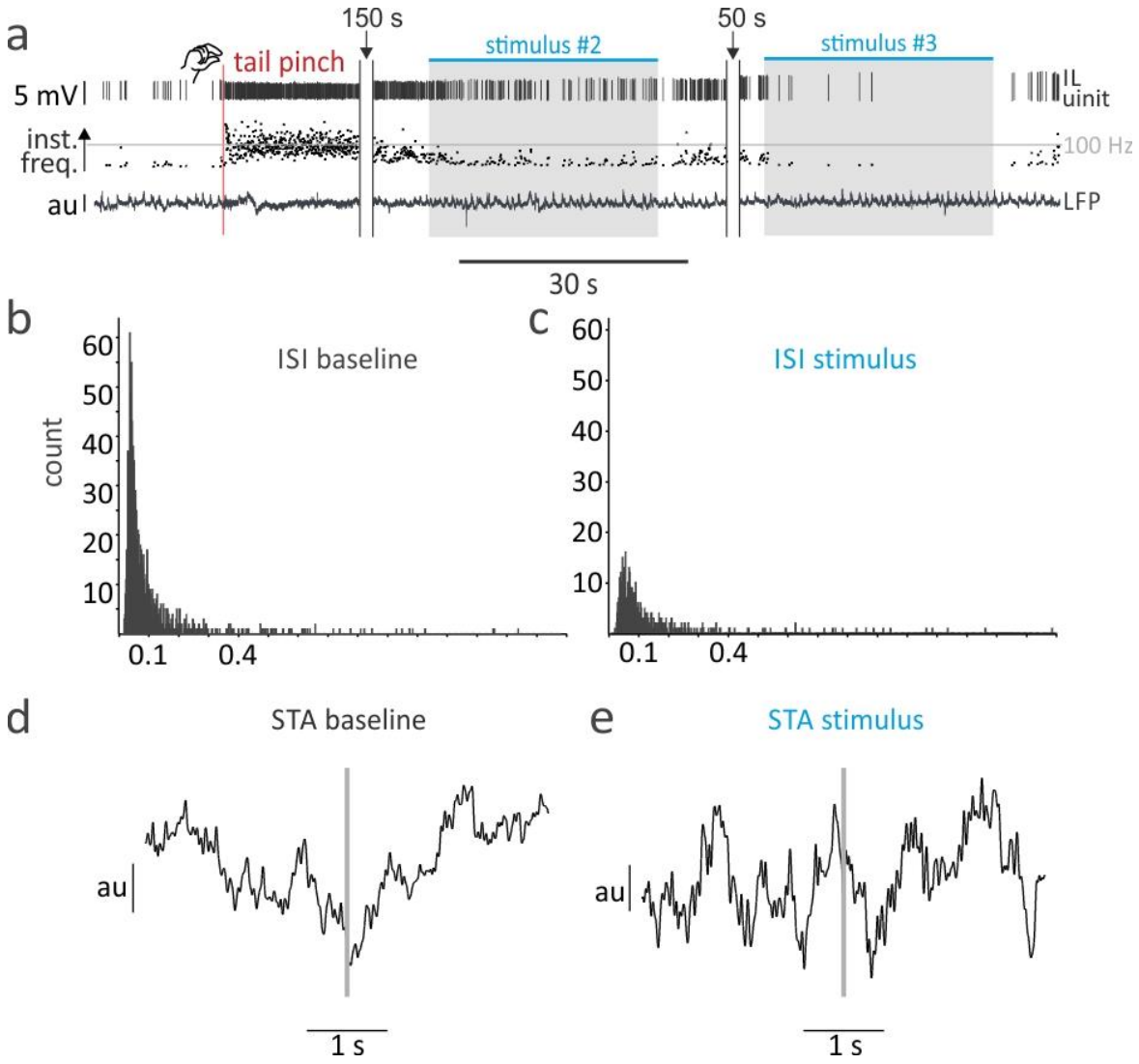

Figure 4.3.2. Photostimulation-induced glycinergic inhibition of a pain-sensitive IL thalamic neuron.

a) Firing pattern of a recorded IL thalamic neuron induced by a painful stimulation (tail pinch). Note the increased activity of the cell immediately after tail pinch, and the inhibitory effect of glycinergic activation that lasts only during the laser illumination. . **b-c)** Inter-spike interval histograms before and during stimulation. **d-e)** Spike triggered averages before and during stimulation. **au** – arbitrary units.

We induced high frequency thalamic firing and desynchronized cortical activity with a tail pinch, as indicated on panel ‘a’ of figure 4.3.2. The first stimulus train was applied 60 seconds after the tail pinch, followed by three more trains separated by 80, 60 and 130 seconds. With every subsequent stimulus train, we decreased the evoked high frequency firing and synchronized the disrupted cortical oscillation. After the offset of each stimulus, the reduced firing rate of the neuron together with the synchronized cortical activity returned to the pre-stimulus state.

In these experiments we showed that the glycinergic input had a strong inhibitory effect on IL thalamic cells. This inhibition induced rhythmic firing that was conveyed to the cortex and evoked oscillating activity in the thalamocortical system, putatively involving more and more areas. The effect was immediate and lasted only during the laser stimulation. We did not observe any long-lasting changes in the overall state of the cortical activity. To draw any conclusion about the effect of the glycinergic input on the in vivo *activity of the thalamus, further experiments are needed.*

4.4 Activation of the pathway in freely moving animals

As it was described in the previous section, selective activation of the glycinergic pathway in anaesthetized animals induced rhythmic firing in tonically-active TC cells, and synchronized TC activity after a desynchronizing painful stimulus. The evoked oscillatory activity in the cortex had increased power in the slow (1-6) frequency range. Considering the fast, strong and reliable effect of the inhibition, and the fact that the altered features of thalamocortical activity are also affected by the aforementioned ascending activating system, it is reasonable to ask if this prominent ascending inhibition had any behavioral manifestation.

To investigate this question, we used the previously described GlyT2::cre transgenic strain with transfected glycinergic neurons (n = 7). We implated screw electrodes over the ipsi- and contralateral frontal and parietal corticies to monitor changes in cortical activity during behavior, and an optic fiber into the ipsilateral IL to deliver laser pulses (Fig. 4.4.1).

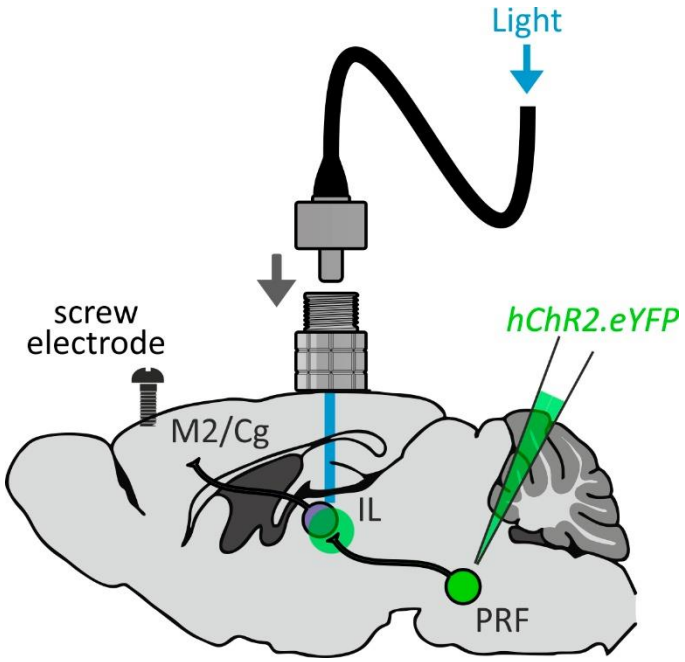

Figure 4.4.1. Electrode arrangement for the activation of the glycinergic fibers in the IL thalamus in freely behaving animals.

After implantation, animals were left to recover from surgery for one week. Following the recovery period the optical fiber and the recording cable were connected 30 minutes before each recording session. During this 30 minutes, animals were kept in their homecage to get used to the wires and move naturally. After 30 minutes, mice were placed in a 42 x 52 cm open arena to test the effect of the activation of the glycinergic pathway on their behavior. One recording session usually lasted for 50-60 minutes and 5-10 stimuli were applied.

In the arena at the begining of the sessions, mice spent most of their time near the walls, and as they got used to the environment they started to explore it. We delivered 30-seconds-long stimuli at 30 Hz first systematically separated by 5 or 10 minutes, and then at random times to avoid the effect of expectation caused by the patterned stimulus. No difference between these two paradigms could be found. During each stimulus we observed reduced bradykinetic motion, but the animals did not seem to loose consciousness, fall asleep or show freezing behaviour. To characterize the effect of the stimulus and to quantify the reduction in motion, we calculated the distance travelled by the animals during stimulated versus non-stimulated periods. The distance travelled was normalized to the distance travelled during the whole

session. We observed a 30.88% ± 4.68% reduction (n = 9 animals, Wilcoxon signed rank test, p = 0.008) in distance travelled compared to the pre-stimulus period (Fig. 4.4.2 a).

To better understand the nature of the evoked behavioral response and the network behind it, we tested if decreasing the power of the illumination (and thus the amount of glycinergic fibers activated) would evoke a graded response, or if the phenomenon is an all-or-none event. When we used maximal laser power, in most cases the animal showed complete behavioral arrest. Depending on the exact location of the optic fiber relative to the glycinergic terminals, the movement reduction varied among animals. When we reduced the intensity of the illumination, the distance travelled increased compared to the maximal intensity stimulation (Fig. 4.4.2 b), but instead of moving straight ahead, the animal turned contralaterally to the side of stimulation.

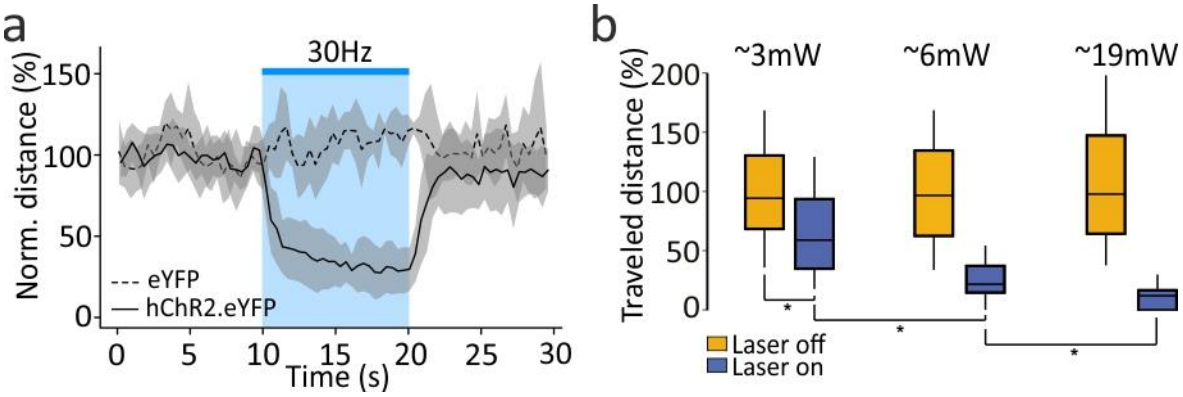

Figure 4.4.2. Behavioral effects of the photoactivation of glycinergic fibers.

a) Decreased distance travelled during 30 Hz activation of the glycinergic fibers in virus-injected compared to control animals. **b)** Gradual decrease of distance travelled with increasing laser intensities.

Together with the behavioral changes, we also monitored the parallel transitions in cortical activity. During exploratory behavior, as expected, we recorded high frequency asynchronous activity with small amplitude. Once the stimulation began, the increased dominance of slow frequency ranges could be detected on the wavelet transform, which was persistent during the whole stimulation. After the stimulus offset, both the altered cortical activity and behavior returned to the pre-stimulus state (Fig. 4.4.3). Note that this was also

the case regarding the firing pattern of the thalamic unit and the parallel cortical activity described previously in anaesthetised animals.

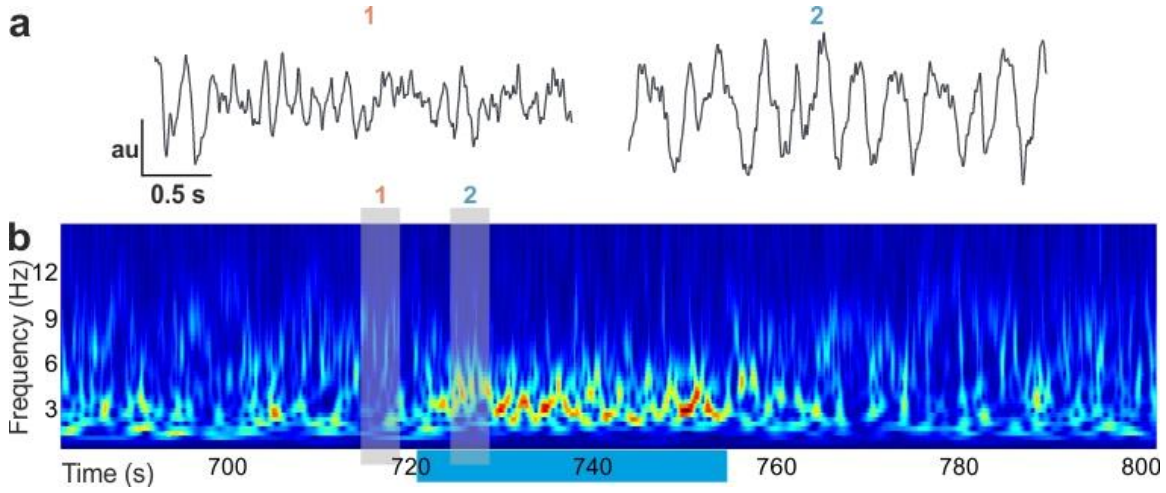

Figure 4.4.3. Cortical activity during stimulation in freely behaving animals.

a) Example traces of cortical LFP before (1) and during (2) photostimulation. **b)** Changes in the dominant frequency range of cortical activity before and during stimulus shown on a wavelet transform. Note the transient increase of slow frequencies in the signal.

To compare the effect of the stimulation on cortical activity across sessions, we standardized the LFP signal and then calculated the power spectra during and before each stimulation. In these power spectra pairs, we compared the difference in each bin in four animals. On figure 4.4.4 the difference in LFP power between control and stimulated conditions is shown in one representative animal. We detected a significant power increase in the bins between 2-6 Hz during stimulation compared to control (Mann-Whitney U-test for stimulation sections and paired control periods, $p < 0.01$)

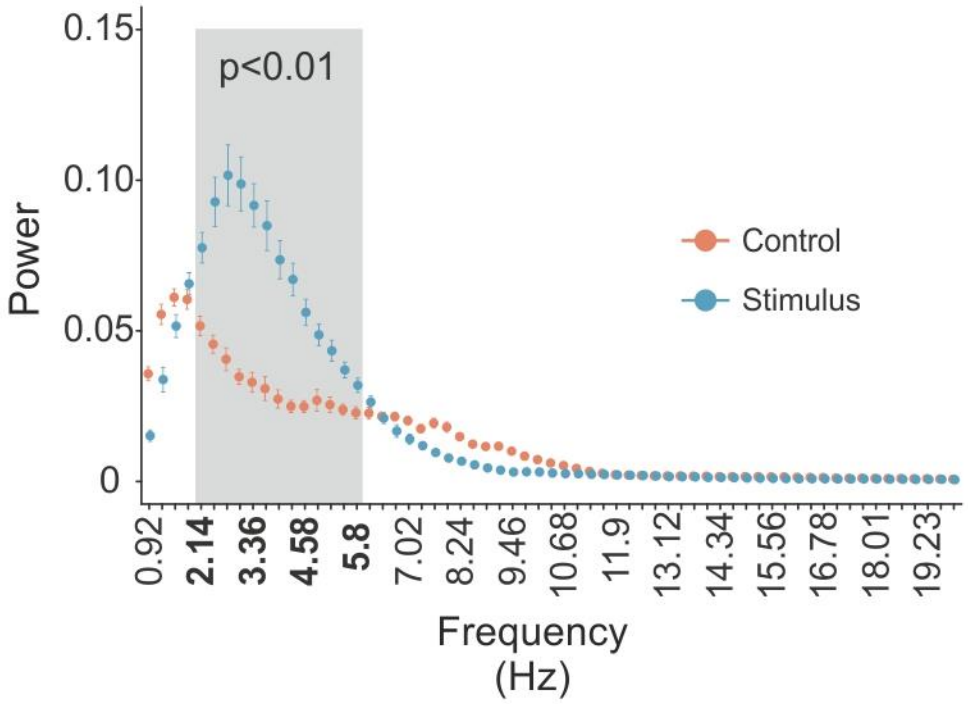

Figure 4.4.4. Power spectrum of the cortical LFP during stimulus and control.

In freely moving experiments, we have shown that, by activating the glycinergic fibers, a prominent behavioral effect could be evoked during which all ongoing behavioural activity was suspended. By gradually decreasing the intensity of the illumination, the effect was also gradually decreased. Parallel to the behavioral changes, altered cortical activity could be detected. Both the behavioral effect and the cortical activity change were transient, lasted only during the stimulation, and no long term state transition was observed. These results, together with the IL thalamic unit recordings in anesthetized animals, imply that the effect of the inhibition is motor-related and conveyed to the cortex via the IL thalamus.

4.5 Cortico-PRF Pathway

In the previous sections, it was shown that the glycinergic inhibition in the IL thalamus can synchronize thalamocortical activity and can induce rhythmic oscillations in the cortex. These findings are consistent with the concept of the sleep-promoting effect of the IL proposed by others (Hunter and Jasper, 1949). The altered activity, however, was associated with prominent movement-related effects that raised the possibility of IL receiving motor signals and playing a role in executing motor plans. In this case we expect afferents from brain regions responsible for motor-related functions.

To address these questions, we used classical and virus-mediated tracing methods. First, in order to identify the origin of the afferents, we injected fluorogold as a retrograde tracer into the PRF (n = 4). We found backlabeled neurons in L5 frontal cortical motor regions (secondary motor and cingulate corticies, M2 and Cg respectively) spanning large anteroposterior areas (Fig. 4.5.1).

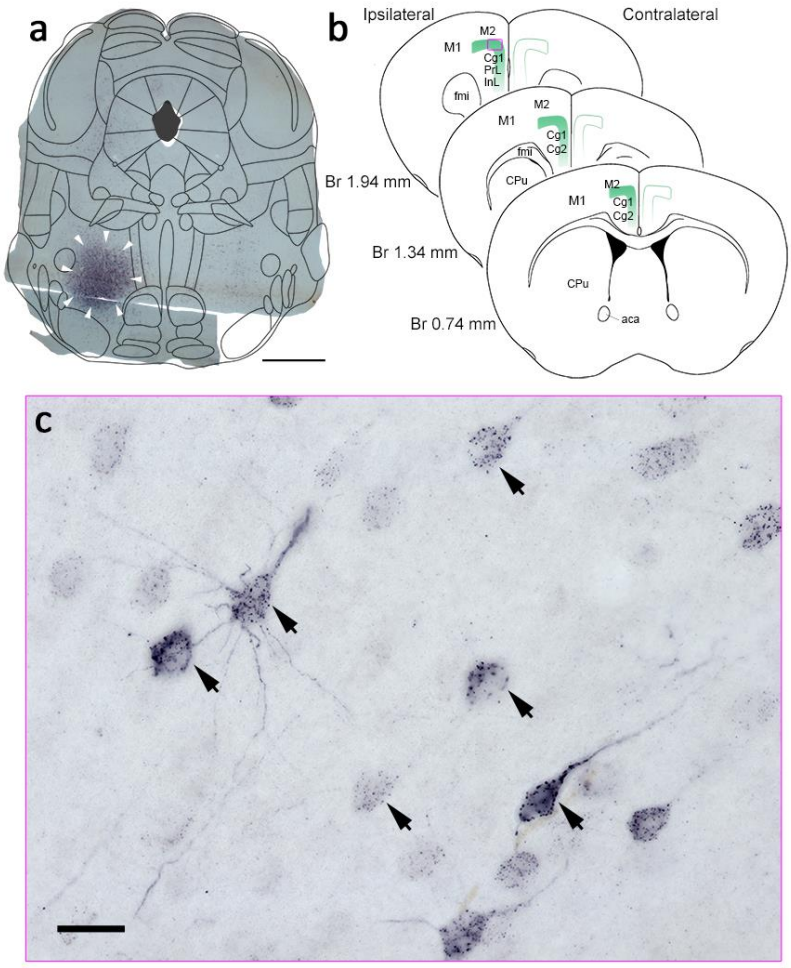

Figure 4.5.1. Retrograde tracing from PRF.

a) Injection site in the PRF. **b)** Distribution of retrogradely-labeled neurons in frontal cortical motor areas. Note the large rostrocaudal spread of the backlabeled cells. **c)** Retrogradely backlabeled neurons (arrows) in M2 (magenta rectangle on panel **b**). Scale bars: 1 mm (panel **a**), 20 mm (panel **c**).

To map the projection pattern of these cortical regions in the brainstem, we injected a cre-dependent virus construct into the previously retrogradely backlabeled cortical areas in RbP4::cre/GlyT2::eGFP double transgenic animals, as described in detail in the methods section (Fig. 4.5.2). Briefly, cortical L5 pyramidal neurons in frontal cortical areas express the retinol binding protein 4 (RbP4), which can thus be used as their selective marker. In this strain we could selectively transfect L5 pyramidal cells in a cre-dependent manner, and also

visualize the glycinergic neurons selectively expressing eGFP and thus showing green fluorescence (Fig. 4.5.3).

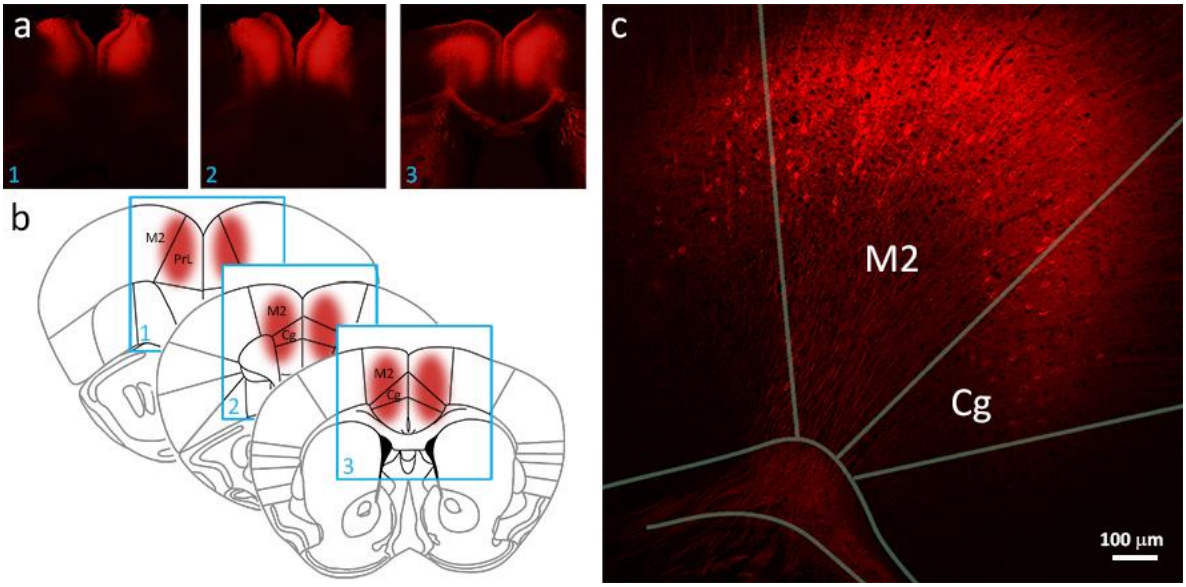

Figure 4.5.2. Virus injection into frontal cortical motor areas in transgenic RBP4::cre/GlyT2::eGFP animals.

a) Fluorescent micrograph of the injection site. **b)** Schematic view and location of the injection site. **c)** Higher magnificiation fluorescent micrograph of the transfected L5 pyramidal neurons in the frontal cortex.

After injecting the virus construct into the frontal cortex (for details see Chapter 3.4.4), we observed massive cortical innervation of several brainstem nuclei (median raphe nuclus, paramedian raphe nucleus) including the PRF and midbrain structures (deep mesencephalic nucleus, periaqueductal gray matter). This indicated that the frontal motor cortical projection to the brainstem is not selective neither to a specific cell type nor to a particular region. Using confocal microscopy we found putative synaptic connections between cortical fibers and PRF glycinergic neurons (Fig. 4.5.3 c). The electron-microscopic validation of these connections is yet to be performed.

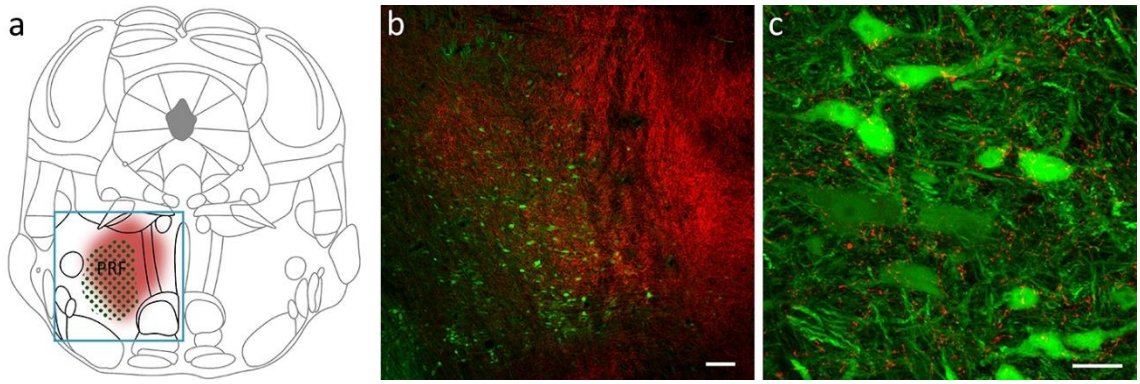

Figure 4.5.3. Transfected frontal cortical fibers in the PRF.

a) Schematic view of the distribution of the transfected fibers relative to the glycinergic cells. **b)** Fluorescent micrograph of the fibers in the PRF **c)** Higher magnificiation fluorescent microgaph of the transfected L5 axons around the glycinergic neurons. Scale bars: 100 μm (panel **b**), 20 μm (panel **c**).

4.6 Spontaneus desynchronization, pharmacological inactivation

In the previous section, we described the morphological characteristics of the cortico-PRF pathway, but its functional properties, like its effect on PRF neuronal activity and on the coupling of cortical oscillations and glycinergic neuronal firing, are still unknown. In order to describe these features, we on the one hand analyzed the spontaneous transitions between different cortical oscillatory activities and the parallel changes in firing pattern of PRF neurons, and on the other hand we experimentally inactivated or stimulated the PRF-projecting cortical cells in ketamine-xylazine anaesthetized animals.

The effect of the anaesthetics is not steady during long recording sessions. This is represented by the changes in the cortical oscillatory pattern. When anaesthesia becomes lighter or more superficial, the cortical slow oscillation will be interspersed with spontaneous desynchronized periods (Fig. 4.6.1 a). We juxtacellularly-recorded PRF neurons and monitored the spontaneous changes in cortical activity. We observed that during slow oscillatory periods, a recorded PRF cell fired the previously-described phase modulated rhythmic AP clusters, but when the slow oscillation was replaced by a desynchronized period, the firing pattern of the PRF cell immediately followed this transition and became tonic (Fig. 4.6.1 a). When the cortical activity was restored, the AP clusters also reappeared. The second

peak on the inter-spike interval histogram, and the large amplitude of the spike triggered average during synchronous cortical oscillations, indicated the rhythmic firing activity of the PRF cell (Fig. 4.6.1 b-e). The parallel changes of the cortical oscillation and neural firing confirmed that the rhythmic pattern of activities observed in the cortex and in the PRF were not independent, but strongly coupled.

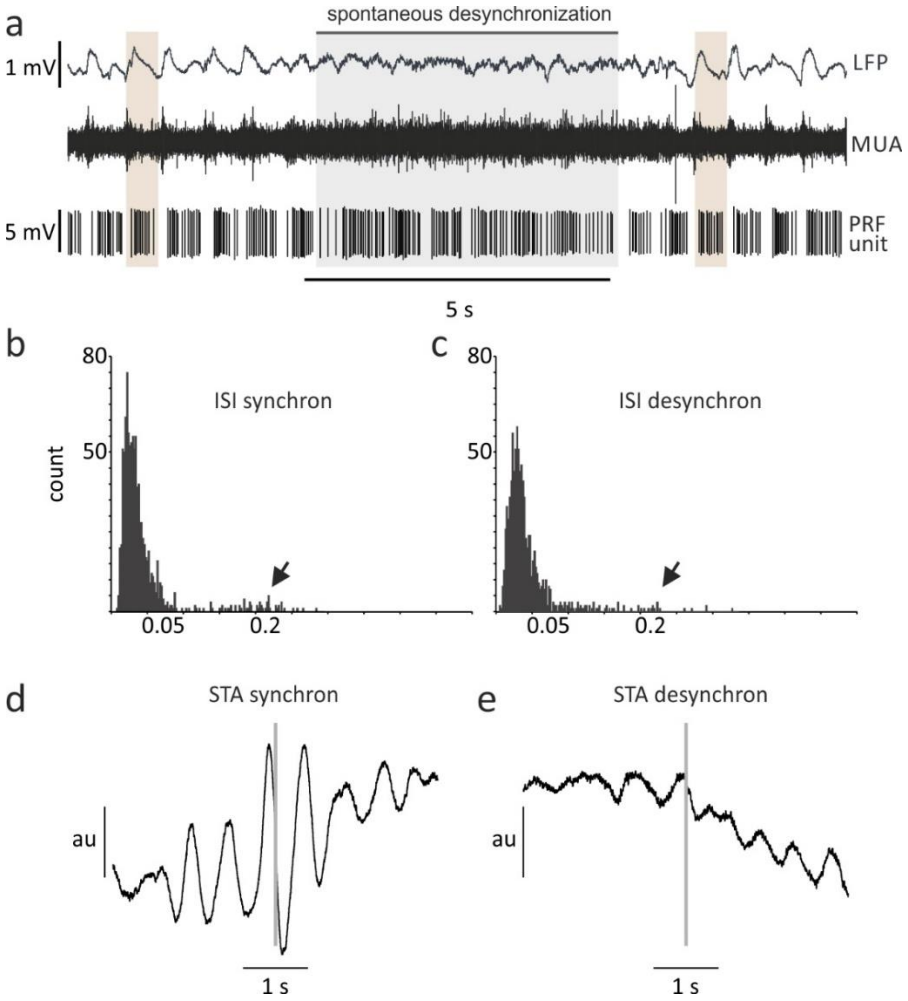

Figure 4.6.1. Spontaneous desynchronization of cortical activity.

a) Spontaneous de- and resynchronization of the cortical slow oscillation and the coupled firing activity of a recorded PRF neuron. Note that during synchronous cortical activity, the PRF neuron fired rhythmic clusters of action potentials and its firing pattern followed the changes in cortical activity. **b-c)** Inter-spike interval histograms of the PRF cell during synchronous and desynchronized cortical activity. Note the second smaller peak in the case of synchronous oscillations. **d-e)** Spike triggered averages during synchronous and desynchronized cortical activity.

To experimentally reproduce changes in cortical activity, we used 2 molar potassium chloride (KCl) to induce cortical spreading depression (CSD) in the frontal motor regions. Although the spontaneous desynchronization and the induced CSD might look similar in the LFP signal, it is important to note that while in the former case cortical neurons are asynchronously active, in the later condition they do not fire at all, and thus PRF neurons do not receive cortical input.

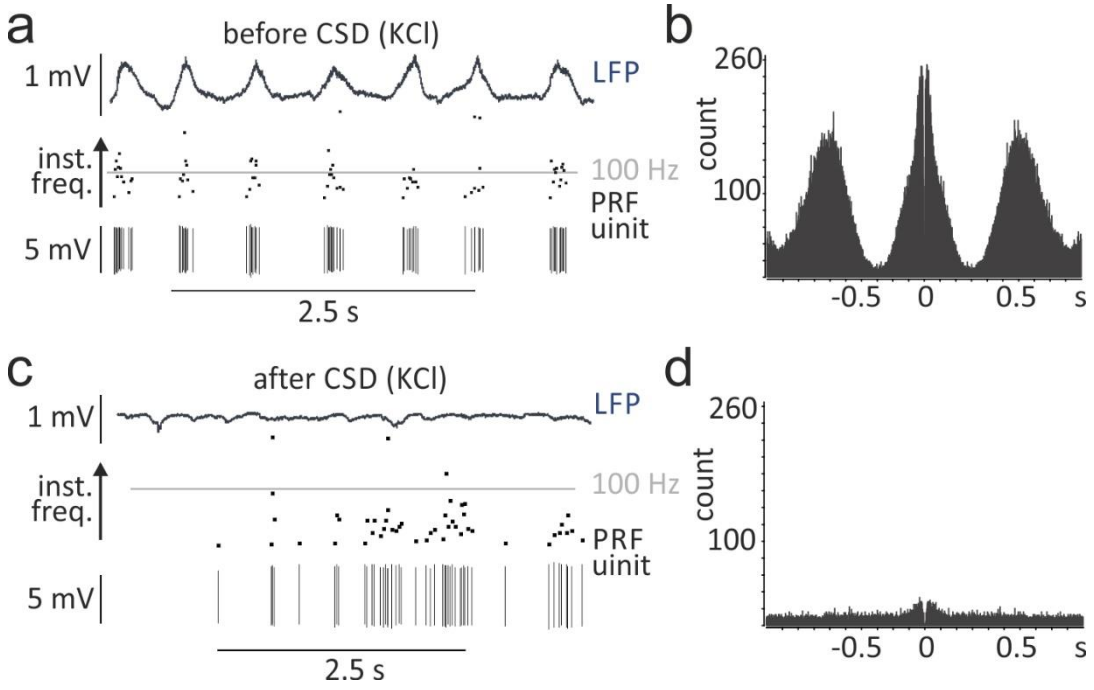

Figure 4.6.2. Effect of cortical spreading depression (CSD) on PRF activity.

a) Representative example of the baseline activity of a PRF neuron. Note the AP clusters. **b)** Autocorrelogram before CSD. **c)** Firing pattern of the PRF cell after the application of 2 molar KCl on the surface of the cortex. The rhythmic firing pattern was replaced by an irregular activity. **d)** Autocorrelogram during CSD.

During the application of KCl, PRF cells became non-rhythmic and decreased their firing rate (Fig. 4.6.2, 4.6.3).

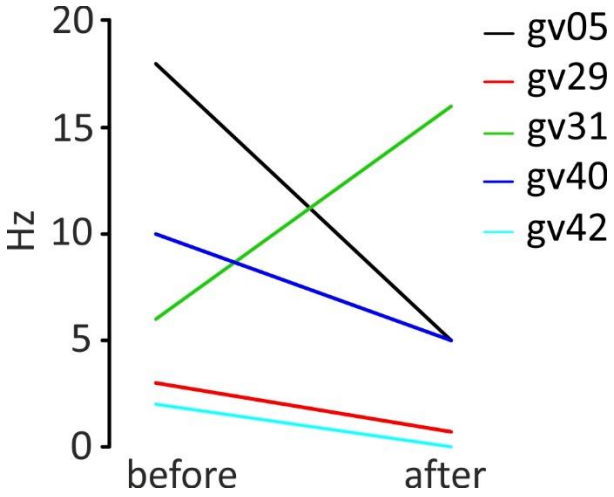

Figure 4.6.3. Effect of cortical inactivation on the firing rate of glycinergic cells.
Note that the firing rate of a recorded anti-phase neuron (gv31, cell #6 in Fig 4.2.3) was increased.

After wash–out of KCl, cortical activity slowly recovered and was followed by the partial recovery of PRF firing. These results indicate that PRF cells gain their rhythm from the synchronized firing of cortical pyramidal cells, but show activity without synchronous cortical input. It is important to note, however, that we did not eliminate all the cortical excitation by CSD, not to mention other sources of excitation.

4.7 Electrical and optical activation

After observing the effect of spontaneous desynchronization and inactivation of the cortex on PRF neural activity, we tested the efficacy of the cortico-PRF pathway by stimulating the cortex and monitoring the response of the PRF cells in anaesthetized animals. First we applied electrical stimulation (1-2 μA) using a bipolar stimulating electrode on the surface of the cortex. By this we activated a complex cortical network involving several cell types. This activation resulted in a L5 output signal descending to the PRF that excited the innervated glycinergic cells.

We found that the glycinergic neurons (n = 4) faithfully followed electrical stimulation with short (10 ms) latency at 1 Hz. Increasing stimulation frequency caused the response probability to became more variable (Fig. 4.7.1).

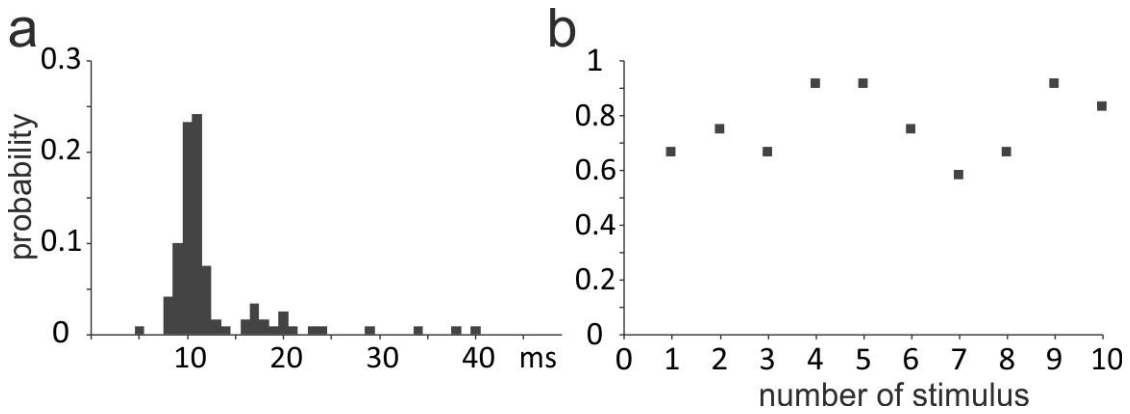

Figure 4.7.1. Response of PRF cells to electrical stimulation of the cortex.

a) Population PSTH of four glycinergic cells during stimulation at 1 Hz. Note that the majority of the responses occur with high probability around 10 ms after the stimulus. **b**) Population response probability within a 20 Hz train. Note that the probability of the response remains high within the train.

In the RBP4::cre\GlyT2::eGFP strain, we labeled the L5 pyramidal neurons and made them express the ChR2 molecule so that we could use light to activate them selectively. Compared to electrical activation, in this case we primarily excited L5 neurons (the output layer of the cortex) so that the effect was more direct. We used 5-ms-long pulses on the surface of the brain with ~1300 mW/mm^2 intensity. To keep the brain surface hydrated, we built a chamber around the craniotomy and filled it with saline. The tip of the optic fiber was dipped into the saline. The recorded glycinergic cells in the PRF, just like in the case of electrical stimulation, followed the pulses with short latency and decreasing reliability with increasing frequency (Fig. 4.7.2).

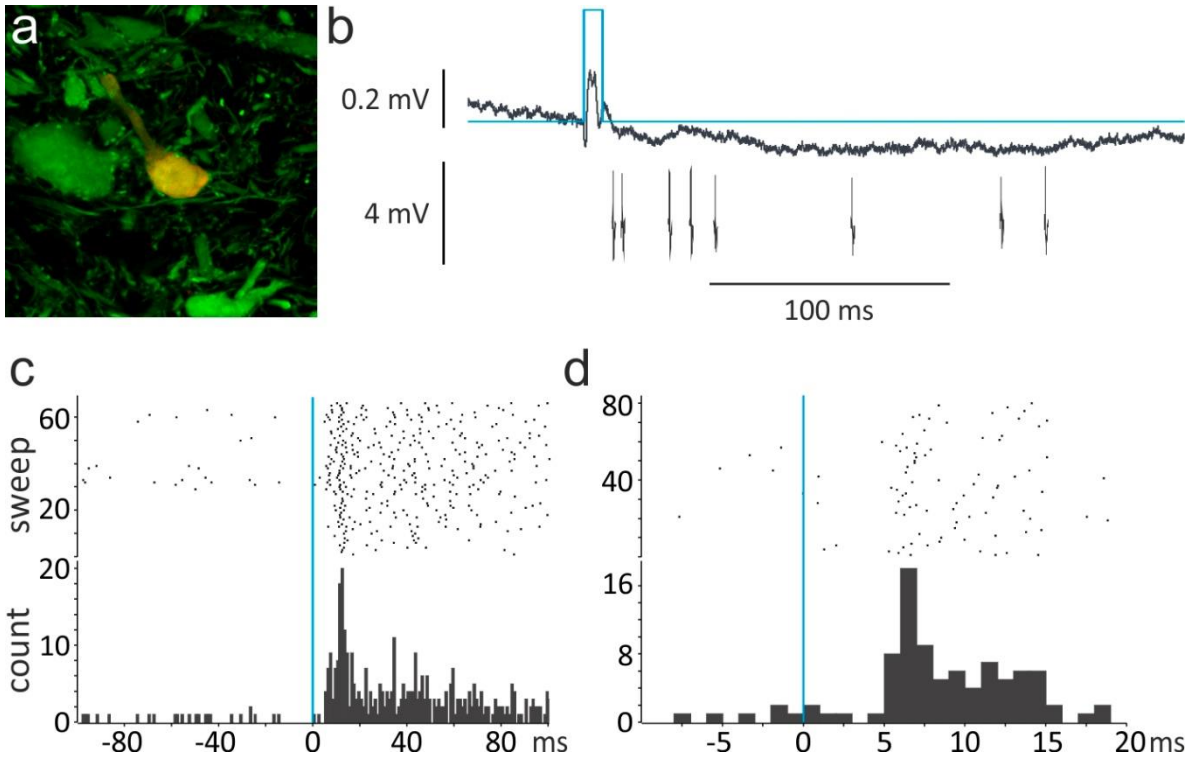

Figure 4.7.2. Optical activation of L5 pyramidal cells in a transgenic animal.

a) Fluorescent micrograph of a recorded and labelled glycinergic cell in the PRF. **b)** Evoked cortical response and cell firing by a single laser pulse. **c-d)** Peri-stimulus time histograms at 1 and 10 Hz, respectively. On the raster plot (upper part of the figures) each dot represents an AP, which are aligned to the stimulus (blue line). Note the short latency response of the PRF cell.

These data (spontaneous desynchronization, inactivation and stimulation of the cortex) showed that glycinergic neural activity is strongly affected by cortical input, and that we could change the firing pattern of PRF cells either by activation or inactivation of the PRF-projecting cortical cells. To deeply analyze the properties of altered PRF firing caused by changes in cortical activity, further experiments need to be performed.

Part II – Integration in the thalamus

4.8 Integration in the thalamus - convergence of driver inputs on a single TC neuron

In the following section I am going to describe a different aspect of thalamic operation. As it was described in Chapter 1.7, excitatory driver inputs in the thalamus can have both subcortical (classic relay nuclei) and cortical L5 origin. The relative distribution of these drivers was mapped in the whole primate thalamus (Rovó et al., 2012). This study showed that besides *first order* thalamic regions innervated by subcortical *drivers* only and *higher order* regions innervated by cortical drivers, there were *convergent* regions where the two *driver* inputs colocalized. In primates, however, functional experiments to uncover the role of the separation and convergence of *drivers* with different origins in organizing thalamocortical information processing cannot be performed due to both ethical and biotechnological reasons. To investigate these questions, we used rodent models (both rats and mice) and examined the relative distribution and function of the cortical and subcortical *drivers* in the somatosensory system.

Two major somatosensory nuclei can be distingushed in the rodent thalamus (Jones, 1985). One is the *ventral posterior nucleus* (VPM) that receives its *driver* input from the *principal trigeminal nucleus* of the brainstem, and faithfully relays sensory information from the whiskers to the S1 cortex (Deschenes et al., 1998, 2003). Based on these properties, VPM is a classical first order thalamic nucleus. The other somatosensory nucleus is the higer order POm (Fig. 4.8.1), which besides subcortical *drivers* has been shown to also receive driver input from the S1 cortex (Sherman and Guillery, 2001). So, just as in primates, two driver inputs with different origin can also colocalize in the same thalamic area in rodents. These data raise the question of whether the two drivers remain separate at the cellular level in the thalamus or if they might converge onto the same TC cell, allowing higher order nuclei to play a more complex role in sensory information processing than simply relaying the subcortical information to the cortex. In our experiments, we examined the putative existence of convergence both anatomically and physiologically.

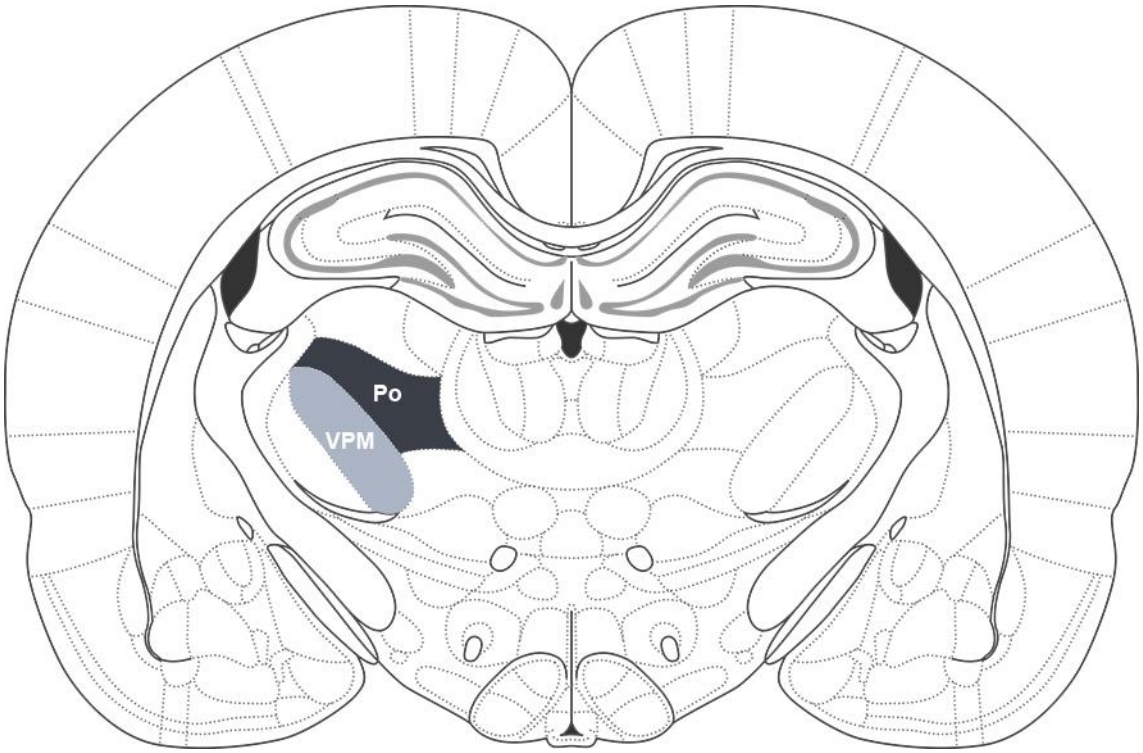

Figure 4.8.1. Somatosensory nuclei of the rodent thalamus.

POm: posterior thalamic nucleus, higher order; VPM: ventral posteriomedial thalamic nucleus, first order.

We labeled the subcortical *drivers* by vGlut2 immunostaining. vGlut2 is known to be selectively expressed in subcortical thalamus-projecting excitatory neurons. Cortical L5 terminals were visualized by anterograde tracing. PHAL (n = 5 mice and n = 6 rats) or BDA (n = 4 rats) was injected precisely to L5 of the S1 cortex. It is important to note that by this method we could not label all the thalamus-projecting L5 cells, and thus only a fraction of the total L5 terminal population was labelled.

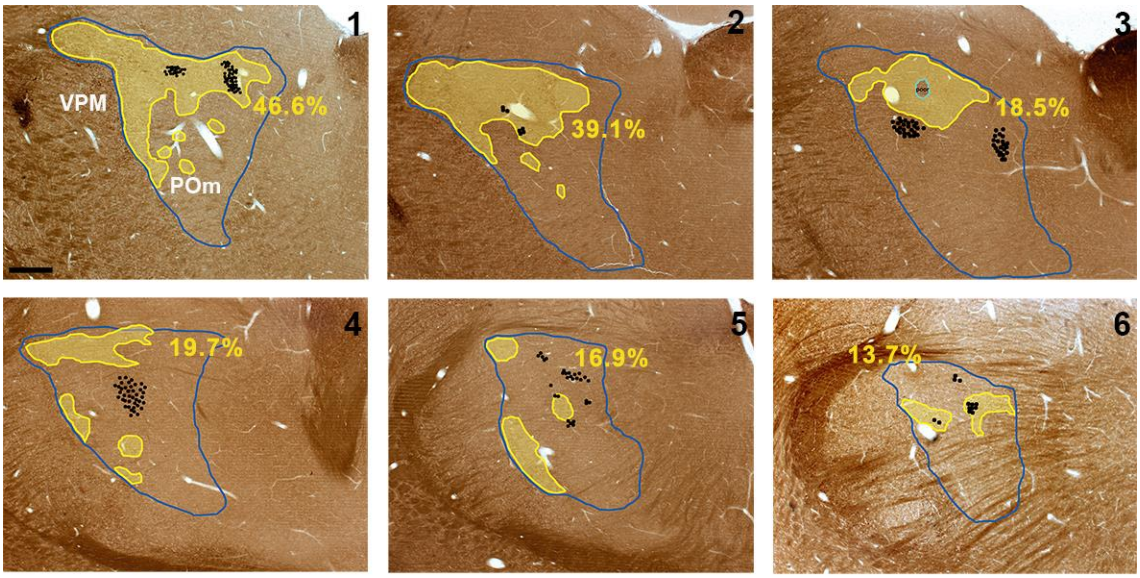

Figure 4.8.2. Distribution of fibers with different origin in the POm at six rostro-caudal levels.

1-6 rostral to caudal. Blue outline: border of POm based on vGluT2 distribution (see Chapter 3.4.4). Yellow shaded area: vGluT2-rich zones within POm. Black dots: large S1 cortical terminals. Percentage represents the fraction of total POm cross-sectional area rich in large vGluT2 terminals.

We found that vGluT2-positive subcortical drivers displayed an inhomogenous distribution in the POm, both in rats and mice. The rostral part of the nucleus was more densely innervated by subcortical drivers, while in caudal regions no or only a few terminals could be observed (Fig. 4.8.2). Based on this inhomogenous pattern, we determined vGlutT2-rich and vGluT2-poor regions (see Materials and Methods) and examined which of these zones were targeted by L5 cortical drivers. We detected large cortical terminals in vGluT2-rich zones, as well as in regions having no or only a few subcortical terminals (Fig. 4.8.2). Within the convergent zones, large cortical and subcortical terminals were in close proximity (Fig. 4.8.3) and measurements on electron-microscopic samples indicated that they both targeted thicker proximal dendritic regions compared to a random sample (Mann-Whitney U test, $p < 2.2e-16$ in both cases, Fig. 4.8.4).

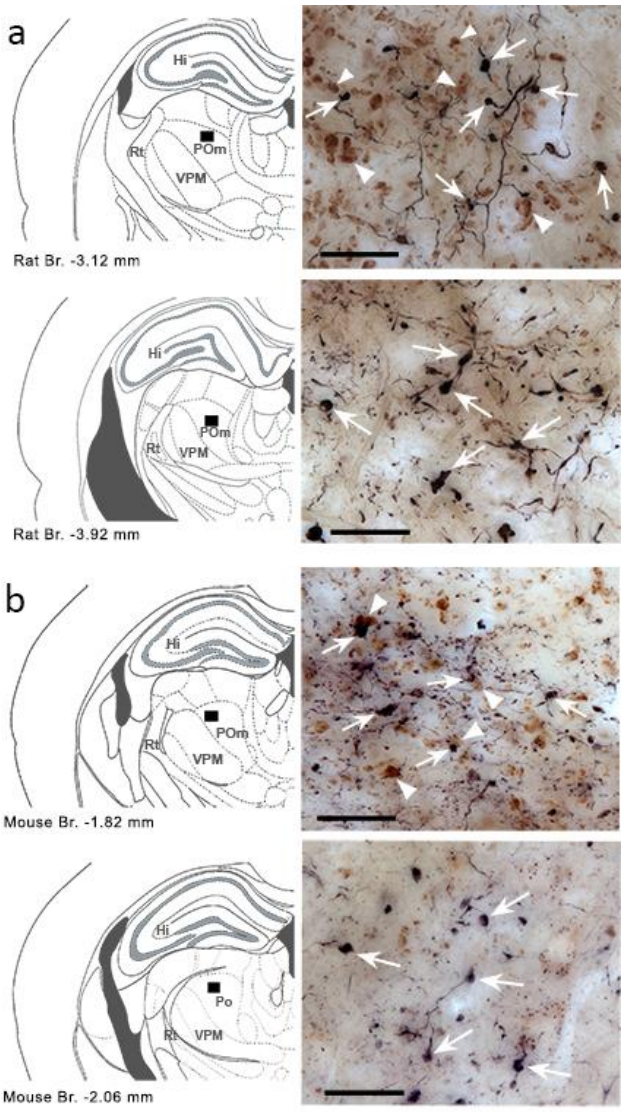

Figure 4.8.3. Putative zones of convergence in the POm of rat and mouse.

a) top: S1 cortical terminals (arrows, black precipitation) in the POm of rats, together with vGluT2-positive subcortical terminals (arrowheads, brown precipitation), bottom: S1 terminals only. **b)** same as panel **(a)** but in mice. Scale Bars: 20 μm.

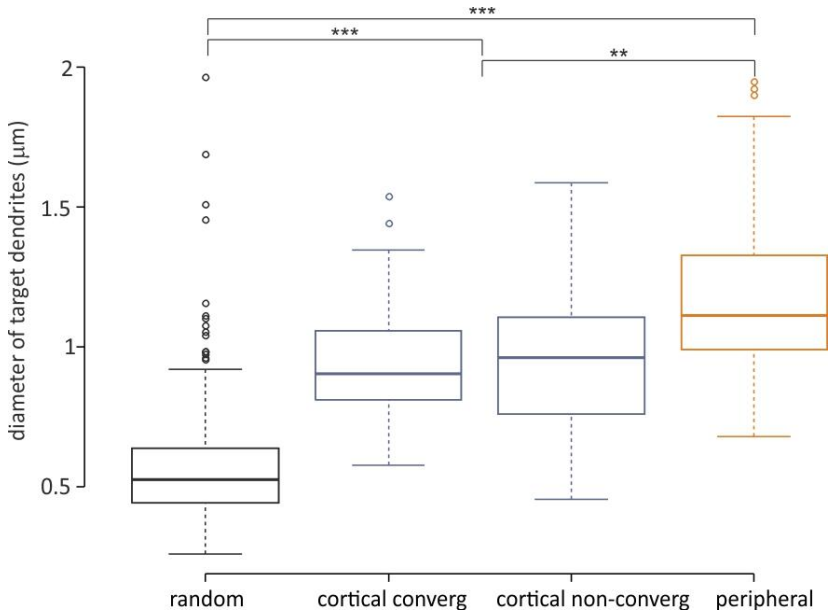

Figure 4.8.4. Distribution of the diameter of the dendritic domains targeted by drivers with different origin compared to randomly sampled terminals.

Randomly sampled terminals targeted significantly thinner dendrites compared to labeled terminals of either cortical or peripheral origin. Boxplots indicate the median, the interquartile range and the minimum and maximum value of the sample. Circles represent outliers (1.5 times of the interquartile range from the 25% and 75% quartile.). We did not find statistical difference between the two groups of cortical terminals (blue boxplots) so the pooled data was used for statistical testing (the significance bars thus point between the two plots).***: $p < 2.2e\text{-}16$, **: $p < 6.899e\text{-}06$.

Correlated light and electron-microscopic analysis also revealed that they could indeed establish synaptic connections with the same thalamic cell.

Besides anatomical evidence, physiological data also support the existance of convergence (Groh et al., 2013). Whisker stimulation, together with optical activation of S1 L5 pyramidal neurons in transgeic mice resulted in a larger evoked response than the linear sum of whisker and cortical stimuli.

In these experiments, we have demonstrated that two driver inputs with different origin can target the same TC neuron. This implies that the firing properties, and thus the transmitted message of these neurons, will be determined by two different information sources and their timing relative to each other.

5 Discussion

In our experiments, we have described a glycinergic-GABAergic pathway originating in the brainstem reticular formation and innervating the IL nuclei of the thalamus. The pathway with similar morphological properties was also identified in humans. Glycinergic-GABAergic fibers ended in large terminals with multiple release sites and formed extremely powerful non-depressing inhibitory connections with the proximal dendrites of TC cells in the IL complex (Fig. 5.2.1). Glycinergic-GABAergic cells in the PRF were shown to fire rhythmic clusters of action potentials coupled to cortical activity. Spontaneous desynchronization, as well as pharmacologically-induced inactivation of the cortex, resulted in a reduced firing rate and disrupted AP clusters in glycinergic neurons, while they were effectively stimulated by the activation of the PRF-projecting cortical cells. In freely moving animals, the selective activation of the glycinergic-GABAergic fibers caused behavioural arrest, or in the case of smaller stimulus intensities, turning movements contralateral to the stimulus.

5.1 Technical considerations

In these experiments we used optical stimulations at 30 Hz for 10 to 30 seconds. Assuming that the PRF-thalamic glycinergic pathway indeed conveys a behavioral stop signal, then its physiological activity can be fundamentally different i.e. both the long-term oscillatory activity in the cortex and the prolonged change in behavior may not be present, or may appear in a different way under physiological conditions. Our results demonstrated the powerful effect of glycinergic inhibition on the activity of the forebrain and raised many functional questions that can only be answerd by performing further specific experiments.

5.2 A novel source of inhibition in the thalamus

In the thalamus, two major sources of inhibition can be differentiated with fundamentally different properties. The GABAergic neurons of the thalamic reticular nucleus are situated as a shell around the thalamus, and their axons homogenously interlace among TC neurons (Jones, 2007). The fibers end in small terminals and form synaptic contacts with the

postsynaptic cells via one or two active zones, without any spatial selectivity in the dendritic domain.

In contrast, extrathalamic inhibition originates from various cell groups (Zi, APT, SNr) located outside of the thalamus (Fig. 5.2.1). These cell groups specifically target particular thalamic regions and form large terminals with multiple release sites selectively on thick proximal dendrites. As it was demonstrated in earlier studies, the IL complex is targeted by several extrathalamic inhibitory nuclei (Bartho et al., 2002; Bokor et al., 2005; Bodor et al., 2008). By discovering the PRF-thalamic pathway, we have described a novel extrathalamic source of inhibition in the IL (Fig. 5.2.1) that shares the morphological and physiological properties of the previously identified ones.

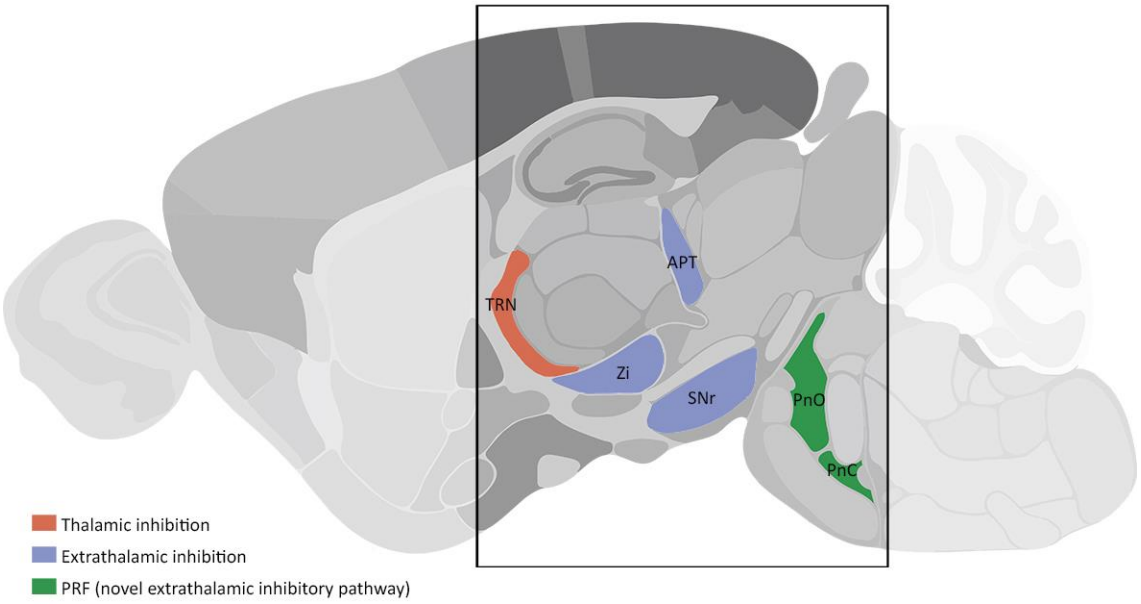

Figure 5.2.1. Thalamic and extrathalamic inhibitory systems

TRN: thalamic reticular nucleus, Zi: zona incerta, APT: anterior pretectum, SNr: substantia nigra pars reticulata, PnO: nucleus pontis oralis, PnC: nucleus pontis caudalis.

The role of the reticular and extrathalamic system in shaping thalamocortical communication and behavior is different, due to their morphological and physiological dissimilarities. The TRN has the ability to exert global inhibition on large thalamocortical networks. However,

its topographic point-to-point connectivity with distinct thalamic cell groups also allows the TRN to act locally in a spatially determined manner. In the temporal dimension, the TRN has a prolonged hyperpolarizing effect, which results in low threshold rebound Ca^{2+} bursts of the thalmic neurons. These bursts activate other TRN cells, and thus the cycle continues and grows, involving larger and larger networks.

The extrathalamic system, however, exerts highly specific spatial and precise temporal connections with the innervated thalamic cells. They do not only target selected nuclei, but also distinct dendritic domains. Their temporal accuracy relies both on the properties of the established synaptic contacts and on the firing rate of the cells.

The spatial-temporal specificity is nicely demonstrated through the feedforward gating of sensory information by the zona incerta (Lavallée et al., 2005). Trigeminal fibers targeting the posterior thalamic nucleus give collaterals to the GABAergic cells of the Zi. The activated incertal cells rapidly and effectively hyperpolarize POm neurons, and thus subcortical excitation cannot evoke action potentials. This effect is localized in POm cells only, and happens with high temporal precision.

The PRF-IL pathway described in this work also shows precise inhibition in the temporal domain. As our experiments demonstrated, high frequency activation of the glycinergic fibers *in vitro* resulted in non-depressing inhibitory postsynaptic currents (IPSCs) on the thalamic cells (Fig. 5.2.2) (Giber et al., 2015). As it was described, PRF neurons fired rhythmic AP clusters in anaesthetized animals with high intra-cluster frequency, suggesting that the non-depressing nature of the synapse has relevance *in vivo*.

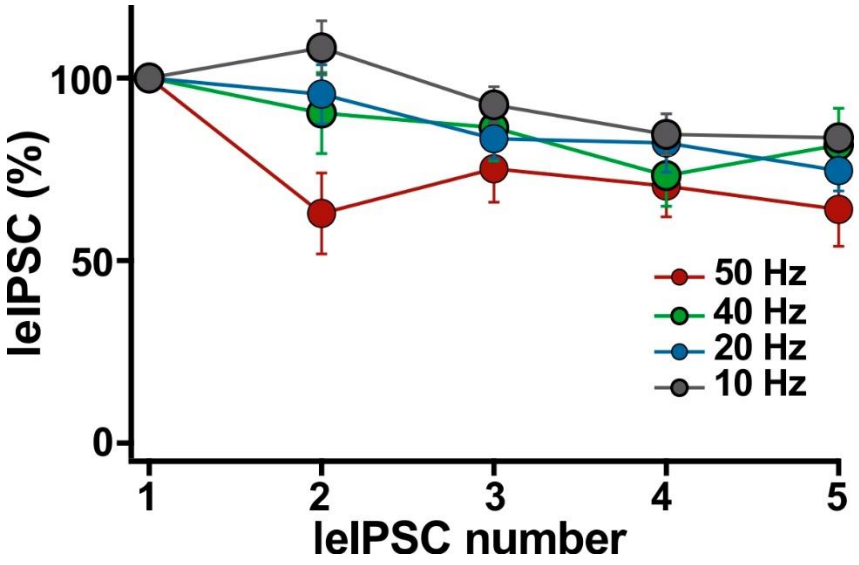

Figure 5.2.2. The nondepressing nature of the PRF – IL glycinergic synapse.

Graph showing light-evoked IPSCs in IL neurons after repetitive photoactivation of the pathway at different frequencies. Note the nondepressing nature of the evoked response even at high frequencies. (Modified from Giber *et al*., 2015).

5.3 Cortical control of the extrathalamic system

High frequency clusters of APs were dependent on cortical activity, as it was demonstrated in Chapter 4.6-4.7, suggesting that rhythmic and synchronous discharge of cortical neurons have a patterning effect on PRF firing. The variability in phase coupling and the presence of anti-phase glycinergic neurons (active during the inactive phases of cortical oscillations) imply the existence of a putative local inhibitory circuit. That is, excitatory cortical fibers activate a group of inhibitory cells in the PRF (phase-coupled glycinergic neurons) that target other glycinergic cells in the PRF and supress their firing for the duration of active cortical periods.

Other extrathalamic inhibitory cell groups were also shown to be under cortical control. GABAergic cells of the Zi receive afferents from descending cortical fibers that regulate their firing in different cortical states. During slow waves, Zi neurons fired at the depth negative („Up state") phases of the cortical oscillation, and during high-voltage spindles they were also tightly coupled to the cortical activity (Barthó et al., 2007).

APT neurons showed heterogenous coherence with the cortical LFP and variable responses to desynchronized cortical oscillations, as predicted by their baseline activity. Neurons with tonic baseline firing showed no noticeable correlation with either synchronous or desynchronized cortical activity, while fast-bursting neurons were modulated by the cortical oscillation, and desynchronized cortical activity resulted in reduced bursting. The most salient cortical coupling was displayed by the slow-rhythmic APT cells. These neurons fired APs related to the cortical „Up states" and their rhythmic activity became irregular upon cortical desynchronization (Bokor et al., 2005).

The representation of cortical activity in extrathalamic inhibitory nuclei implies that their effect on thalmic neurons is partially regulated by cortical commands.

5.4 Participation of the intralaminar thalamus in various tasks

The interpretation of IL function is organized around two main trends. One investigates its role in consciousness, awereness, cognition and sleep/wake regulation, while the other discusses its function in motor processes (see Chapter 1.3). These results are not necessarily contradictory, and can be caused by the heterogeneity of the IL complex in terms of input distribution and targeted areas.

Since the IL is targeted by several components of the reticular activating system (for details see Chapter 1.4 and (Van der Werf et al., 2002)) and projects to frontal cortical areas responsible for higher cognitive precesses, the nonspecific stimulation of these nuclei can indeed support the former idea. On the other hand, different IL nuclei establish connections with the basal ganglia via the striatum (CL and Pf mostly) and frontal cortical motor areas, and thus, depending on the experimental design, motor-related results can also be obtained.

Although little difference can be observed in the density of the glycinergic terminals in IL nuclei, they do not show remarkable preference for any particular nucleus and uniformly innervate the whole complex i.e. this input unites the otherwise divided region. The consequence of this property of the pathway and of the previously-described heterogenous projection is that the selective activation of the glycinergic fibers can lead to combined results.

In freely moving animals, we detected decreased distance travelled and a graded behavioral response (turning movement contralateral to the stimulus, see Chapter 4.4). These effects were strong and immediate, supporting the motor-related function of the glycinergic pathway and IL nuclei, as well as the idea that they play a role in instantanous termination of ongoing behavior. This concept is in accordance with other results, which describe the role of the subthalamic nucleus, the substantia nigra pars reticulata and the striatum in the rapid cancellation of actions (Schmidt et al., 2013). The IL projection to the striatum can participate in this function, although its effect may be more complex. Ellender and colleagues have shown that the excitation from the IL to striatal neurons displays source-dependent differences in synaptic properties. While CL-striatal connections effectively depolarize striatal cells by large amplitude facilitating synapses, Pf-striatal connections play a modulatory role, with small amplitude depressing postsynaptic responses (Ellender et al., 2013).

Besides these movement-related effects, the cortical slow oscillation induced by the activation of the glycinergic fibers allows a different interpretation of the results. During long-lasting laser stimulations, some thalamic cells changed their tonic-like firing and became rhythmic, conveying this synchronous activity to the targetted cortical areas. This putative sleep-regulating effect is in accordance with the connection of IL nuclei with the components of the reticular activating system (Van der Werf et al., 2002) and with previous functional studies (Hunter and Jasper, 1949).

Since the IL nuclei are not uniform, as detailed in other parts of this thesis, the described homogenous glycinergic inhibitory input will have various effects in different nuclei, depending on their connectivity. This may lead to mixed results, but they do not exclude each other. Although the glycinergic input is spatially homogenous in IL nuclei, the temporal properties of the glycinergic cells may specify its role.

5.5 Integration in the thalamus

In our experiments, we mapped the relative distribution of anterogradely-traced S1 cortical fibers and immunolabelled trigeminal terminals in the somatosensory thalamus of rodents

(rats and mice). Colocalization of these terminals was observed in the *higher order* somatosensory nucleus (posterior thalamic nucleus). Both type of terminals showed the morphological characteristics of a driver input: they established synaptic contacts via multiple release sites onto large caliber proximal dendrites (compared to our random sample). The convergence of drivers with different origin on the same TC cell was shown on correlated light and electron micrographs, and was confirmed by electrophysiological recordings.

With these results we showed a novel form of thalamic information processing, where two essentially different information streams conditionally determined the activity of the TC cell. POm neurons were only able to fire and transmit information to the cortex if the cortical driver signal (evoked by optical stimulation in Thy1::ChR2 transgenic animals) co-occured with the sensory driver signal evoked by whisker deflection (Fig. 5.5.1).

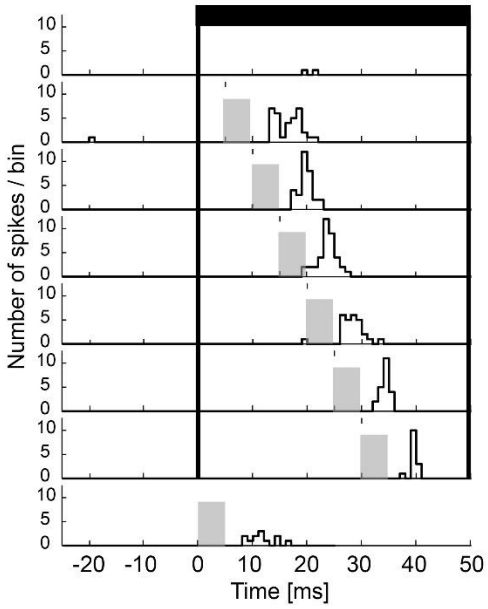

Figure 5.5.1. Evoked activity in POm neurons by co-occuring cortical and sensory signals.

Black rectangle marks the duration of whisker stimulation. Grey bars represent optical stimulation in the cortex. Note the low number of evoked APs under whisker only (top row) and cortex only (bottom row) conditions. The response was increased by the application of paired stimulation (6 middle rows) with different delays. (Modified from Groh *et al*., 2013).

6 Conclusions

6.1 Short- and mid-term goals

Our primary and short-term goals at the behavioral level are to figure out how glycinergic neurons of the PRF can regulate actions via different nuclei of the IL thalamus i.e. to identify the situations during which they are activated. To do so we are planning to record the activity of these cells in freely moving animals using tetrodes. By optically tagging glycinergic neurons in GlyT2::ChR2 transgenic animals or in transfected glycinergic cells of GlyT2::cre mice, we can reliably identify the recorded units.

According to our results, the rhythmic activity of the PRF glycinergic cells is generated by cortical input, supposedly via local inhibitory connections. Assuming that the cortical motor command is necessary for the glycinergic cells to induce behavioral arrest, we should be able to prevent such an effect by the inhibiton of cortical fibers in the PRF. By injecting a cre-dependent halorhodopsin-containing virus construct into the PRF in the previously used Rbp4::cre/GlyT2::eGFP animals, we aim to transfect the cortical cells and inhibit their activity under specific conditions. In animals trained to instantaneously switch between tasks after a sensory cue, we may test if the behavioral switch can be negated by preventing the motor signal from reaching the glycinergic cells.

6.2 Perspectives

Besides the IL nuclei, glycinergic cells of the PRF target other brain areas as well (Zeilhofer et al., 2005). The basal forebrain receives a dense glycinergic innervation, and the inhibition of these neurons can also result in behavioral arrest (Mayse et al., 2015). To demonstrate that the effect of the glycinergic activity indeed emerges via the IL nuclei, loss of function studies are essential. In such experiments, we aim to selectively block the information transfer in the IL during a behavioral switch task, and thus prevent the stop signal transmitted by the glycinergic fibers from reaching the downstream targets of the IL. The striatum, as one of the target areas of the IL nuclei, was shown to play an executive role both in the initiation and termination of movements. To act so, it needs patterned activity from the IL that selects either its movement-initiating or -terminating network (Ding et al., 2010; Thorn and

Graybiel, 2010). If the specific activity of the IL is blocked, then striatal neurons do not receive the signal needed to stop the behavior of the animal.

To perform these experiments, we need to selectively interact with the striatum-projecting IL cells innervated by the glycinergic fibers. This is possible thanks to commercially available transgenic mouse lines expressing the cre enzyme specifically in IL neurons (Wada et al., 1990; Nishiyori et al., 1998; Sunnemark et al., 2005). By the long term optical hyperpolarization of IL cells using step function opsins, the transmission of patterned activity caused by the glycinergic inhibition can be blocked.

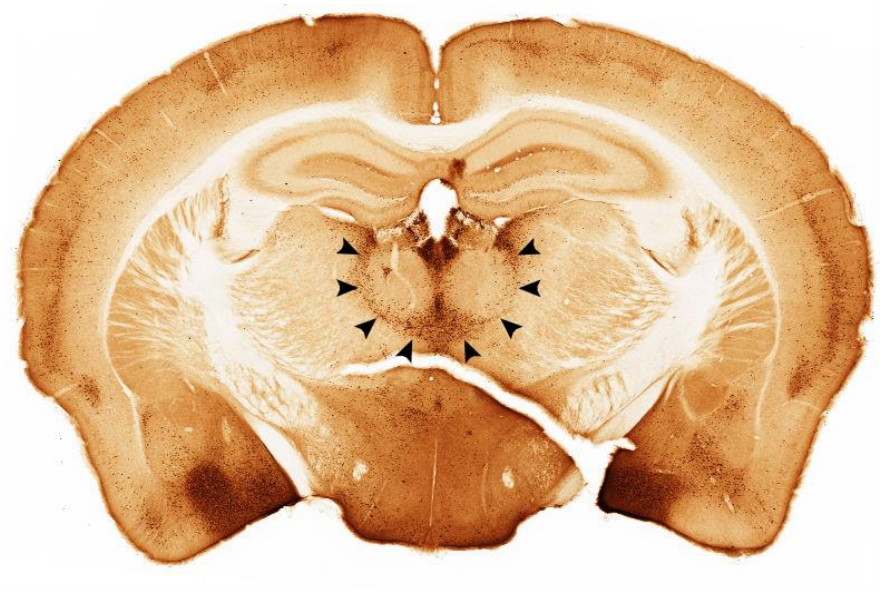

Figure 6.2.1. IL neurons expressing the cre enzyme in the MR89-CRE mouse line
Source: http://www.gensat.org/imagenavigator.jsp?imageID=90667

In some cases, we observed painful stimulus-induced firing of the glycinergic cells. As they project to the IL thalamus, which is part of the medial pain pathway, the observed increased firing and IL inhibition can serve as an internal analgesic system. This opens new perspectives in the examination of the glycinergic cells of the PRF.

Summary

In my thesis I have examined two different aspects of thalamic information processing: first, the role of an extrathalamic glycinergic inhibitory pathway selectively innervating the intralaminar (IL) nuclear complex, and second, the convergence of two "driver" inputs conveying subcortical and cortical messages on one thalamic neuron in the somatosensory system of rodents.

Besides the general source of inhibition in the thalamus provided by the GABAergic cells of the thalamic reticular nucleus, extrathalamic inhibitory inputs are also present in particular thalamic regions. We found that in the case of the IL the source of the mentioned extrathalamic glycinergic pathway was located in the brainstem in the pontine reticular formation (PRF). Under anaesthesia, the PRF glycinergic cells exerted powerful and rhythmic inhibition to the IL and their firing was coupled to different phases of the frontal motor cortical oscillatory activity. Under freely moving conditions, this inhibition had prominent behavioral manifestations: selective stimulation of the pathway terminated ongoing activity, stopped the movement of the animal and generated slow oscillations in frontal cortical motor regions for the duration of the stimulus. PRF glycinergic neurons showed sensitivity to changes in cortical activity.

The convergence of driver inputs on one thalamic neuron is a new phenomenon that changes the classical view that the only role of the thalamus is to relay sensory information conveyed by subcortical "drivers". We found that in a specific part of the rodent somatosensory thalamus (*posterior nucleus of the thalamus*, POm), that is a so-called "higher order" region, sensory subcortical and already-processed cortical information together determine the message to be transmitted by the thalamocortical neurons.

Összefoglalás

PhD dolgozatomban a talamikus információ feldolgozás két, -serkentő és gátló- aspektusát vizsgáltam. Tanulmányoztam egy az intralamináris talamusz magokat szelektíven innerváló, extratalamikus, glicinerg, gátló pálya szerepét, valamint, egy szenzoros, és egy kérgi információt szállító, serkentő, "driver" bemenet egy sejten való konvergenciáját, rágcsáló szomatoszenzoros talamuszában.

A talamikus gátlás általános, a talamikus retikuláris mag GABAerg sejtejei által közvetített forrása mellett, egyes talamikus magokban kívülről érkező (ún. extratalamikus) gátló bemeneteket is találunk. Az IL magok esetében egy ilyen, az említett extratalamikus, glicinerg pálya, mely az agytörzsi hálózatos állományból ered. Az itt lévő glicinerg sejtek hatékony, ritmikus gátlást közvetítenek az IL magokba, és aktivitásuk altatásban kapcsolt a frontalis motoros kérgi régiók oszilláló működéséhez. Szabadon mozgó állatokban a glicinerg pálya szelektív stimulálása erőteljes viselkedésbeli hatást eredményez: minden folyamatban lévő cselekvés megszakad, az állat felhagy a mozgással. Ezek mellett, a stimulus ideje alatt a frontalis motoros kérgi régiókban megerősödik a lassú oszcillációs aktivitás. Az agytörzsi glicinerg sejtek érzékenyen reagálnak a kérgi aktivitásban bekövetkező változásokra.

A különböző eredetű "driver" bemenetek konvergenciája egy talamusz sejten egy új módja a talamikus információ feldolgozásnak, amely megváltoztatja az eddig kialakított klasszikus elképzelést, mely szerint a talamusz a kéreg alatti "driver"-ek által közvetített szenzoros információt relézi a kéregbe. Eredményeink szerint, rágcsáló szomatoszenzoros talamuszának ún. magasabb rendű magjában (*posterior nucleus of the thalamus*, POm), a szenzoros kéreg alatti, és a már feldolgozott kérgi információ együttesen határozza meg a talamusz sejt által közvetítendő üzenetet, és a szenzoros információ önmagában nem továbbítódik.

Bibliography

A. Earl Walker, Walker AE (1936) An experimental study of the thalamo-cortical projection of the macaque monkey. J Comp Neurol 64:1–39.

Bartho P, Freund TF, Acsady L (2002) Selective GABAergic innervation of thalamic nuclei from zona incerta. Eur J Neurosci 16:999–1014.

Barthó P, Slézia A, Mátyás F, Faradzs-Zade L, Ulbert I, Harris KD, Acsády L (2014) Ongoing network state controls the length of sleep spindles via inhibitory activity. Neuron 82:1367–1379.

Barthó P, Slézia A, Varga V, Bokor H, Pinault D, Buzsáki G, Acsády L (2007) Cortical control of zona incerta. J Neurosci 27:1670–1681.

Bickford ME (2015) Thalamic Circuit Diversity: Modulation of the Driver/Modulator Framework. Front Neural Circuits 9:86.

Bodor AL, Giber K, Rovó Z, Ulbert I, Acsády L (2008) Structural correlates of efficient GABAergic transmission in the basal ganglia-thalamus pathway. J Neurosci 28:3090–3102.

Bokor H, Frère SG, Eyre MD, Slézia A, Ulbert II, Lüthi A, Acsády L (2005) Selective GABAergic control of higher-order thalamic relays. Neuron 45:929–940.

Bowery NG, Smart TG (2006) GABA and glycine as neurotransmitters: a brief history. Br J Pharmacol 147 Suppl:S109-19.

Bradfield LA, Bertran-Gonzalez J, Chieng B, Balleine BW (2013) The thalamostriatal pathway and cholinergic control of goal-directed action: interlacing new with existing learning in the striatum. Neuron 79:153–166.

Calabresi P, Maj R, Pisani A, Mercuri NB, Bernardi G (1992a) Long-term synaptic depression in the striatum: physiological and pharmacological characterization. J Neurosci 12:4224–4233.

Calabresi P, Pisani A, Mercuri NB, Bernardi G (1992b) Long-term Potentiation in the Striatum is Unmasked by Removing the Voltage-dependent Magnesium Block of NMDA Receptor Channels. Eur J Neurosci 4:929–935.

Calderon DP, Fremont R, Kraenzlin F, Khodakhah K (2011) The neural substrates of rapid-onset Dystonia-Parkinsonism. Nat Neurosci 14:357–365.

Charpier S, Deniau JM (1997) In vivo activity-dependent plasticity at cortico-striatal connections: evidence for physiological long-term potentiation. Proc Natl Acad Sci U S A 94:7036–7040.

Chauvette S, Crochet S, Volgushev M, Timofeev I (2011) Properties of slow oscillation during slow-wave sleep and anesthesia in cats. J Neurosci 31:14998–15008.

Chen CH, Fremont R, Arteaga-Bracho EE, Khodakhah K (2014) Short latency cerebellar modulation of the basal ganglia. Nat Neurosci 17:1767–1775.

Clascá F, Porrero C, Galazo MJ, Rubio-Garrido P, Evangelio M (2016) Axons and Brain Architecture. Elsevier.

Clascá F, Rubio-Garrido P, Jabaudon D (2012) Unveiling the diversity of thalamocortical neuron subtypes. Eur J Neurosci 35:1524–1532.

Deschenes M, Timofeeva E, Lavallee P (2003) The relay of high-frequency sensory signals in the Whisker-to-barreloid pathway. J Neurosci 23:6778–6787.

Deschenes M, Veinante P, Zhang ZW, Deschênes M (1998) The organization of corticothalamic projections: reciprocity versus parity. Brain Res Brain Res Rev 28:286–308.

Ding JB, Guzman JN, Peterson JD, Goldberg J a, Surmeier DJ (2010) Thalamic gating of corticostriatal signaling by cholinergic interneurons. Neuron 67:294–307.

Ellender TJ, Harwood J, Kosillo P, Capogna M, Bolam JP (2013) Heterogeneous properties of central lateral and parafascicular thalamic synapses in the striatum. J Physiol 591:257–272.

Giber K, Diana MA, M Plattner V, Dugué GP, Bokor H, Rousseau C V, Maglóczky Z, Havas L, Hangya B, Wildner H, Zeilhofer HU, Dieudonné S, Acsády L (2015) A subcortical inhibitory signal for behavioral arrest in the thalamus. Nat Neurosci 18:562–568.

Groh A, Bokor H, Mease R a, Plattner VM, Hangya B, Stroh A, Deschenes M, Acsády L (2013) Convergence of Cortical and Sensory Driver Inputs on Single Thalamocortical Cells. Cereb Cortex:1–13.

Guillery RW, Sherman SM (2002) Thalamic relay functions and their role in corticocortical communication: generalizations from the visual system. 33:163–75.

Herkenham M (1980) Laminar organization of thalamic projections to the rat neocortex. 207:532–5.

Hernandes MS, Troncone LRP (2009) Glycine as a neurotransmitter in the forebrain: a short review. J Neural Transm 116:1551–1560.

Hunter J, Jasper HH (1949) Effects of thalamic stimulation in unanaesthetised animals; the arrest reaction and petit mal-like seizures, activation patterns and generalized convulsions. Electroencephalogr Clin Neurophysiol 1:305–324.

Ichinohe N, Mori F, Shoumura K (2000) A di-synaptic projection from the lateral cerebellar nucleus to the laterodorsal part of the striatum via the central lateral nucleus of the thalamus in the rat. Brain Res 880:191–197.

Jahnsen H, Llinás R (1984) Ionic basis for the electro-responsiveness and oscillatory properties of guinea-pig thalamic neurones in vitro. J Physiol 349:227–247.

Jones EG (1985) The Thalamus (Jones EG, ed). Boston, MA: Springer US.

Jones EG (2007) The Thalamus. Cambridge: Cambridge University Press.

Kinney HC, Korein J, Panigrahy A, Dikkes P, Goode R (1994) Neuropathological Findings in the Brain of Karen Ann Quinlan - The Role of the Thalamus in the Persistent Vegetative State. N Engl J Med 330:1469–1475.

Krout KE, Loewy AD (2000) Periaqueductal gray matter projections to midline and

intralaminar thalamic nuclei of the rat. J Comp Neurol 424:111–141.

Krout KE, Loewy AD, Westby GW, Redgrave P (2001) Superior colliculus projections to midline and intralaminar thalamic nuclei of the rat. J Comp Neurol 431:198–216.

Lavallée P, Urbain N, Dufresne C, Bokor H, Acsády L, Deschênes M (2005) Feedforward inhibitory control of sensory information in higher-order thalamic nuclei. J Neurosci 25:7489–7498.

Le Gros Clark WE (1932) The Structure and Connections of the Thalamus. Brain 55:406–470.

Liu QR, López-Corcuera B, Mandiyan S, Nelson H, Nelson N (1993) Cloning and expression of a spinal cord- and brain-specific glycine transporter with novel structural features. J Biol Chem 268:22802–22808.

Mayse JD, Nelson GM, Avila I, Gallagher M, Lin S-C (2015) Basal forebrain neuronal inhibition enables rapid behavioral stopping. Nat Neurosci advance on.

McIntire SL, Reimer RJ, Schuske K, Edwards RH, Jorgensen EM (1997) Identification and characterization of the vesicular GABA transporter. Nature 389:870–876.

Morales I, Sabate M, Rodriguez M (2013) Striatal glutamate induces retrograde excitotoxicity and neuronal degeneration of intralaminar thalamic nuclei: their potential relevance for Parkinson's disease. Eur J Neurosci 38:2172–2182.

Nishiyori A, Minami M, Ohtani Y, Takami S, Yamamoto J, Kawaguchi N, Kume T, Akaike A, Satoh M (1998) Localization of fractalkine and CX3CR1 mRNAs in rat brain: does fractalkine play a role in signaling from neuron to microglia? FEBS Lett 429:167–172.

Pereira de Vasconcelos A, Cassel J-C (2015) The nonspecific thalamus: A place in a wedding bed for making memories last? Neurosci Biobehav Rev 54:175–196.

Pinault D (1996) A novel single-cell staining procedure performed in vivo under electrophysiological control: morpho-functional features of juxtacellularly labeled thalamic cells and other central neurons with biocytin or Neurobiotin. J Neurosci

Methods 65:113–136.

Rao JS (1976) Some Tests Based on Arc-Lengths for the Circle. Indian J Stat Ser B 38:329–338.

Rodriguez-Sabate C, Llanos C, Morales I, Garcia-Alvarez R, Sabate M, Rodriguez M (2014) The functional connectivity of intralaminar thalamic nuclei in the human basal ganglia. Hum Brain Mapp 36:1335–1347.

Rovó Z, Ulbert I, Acsády L (2012) Drivers of the primate thalamus. J Neurosci 32:17894–17908.

Sagné C, El Mestikawy S, Isambert M-F, Hamon M, Henry J-P, Giros B, Gasnier B (1997) Cloning of a functional vesicular GABA and glycine transporter by screening of genome databases. FEBS Lett 417:177–183.

Schiff ND, Giacino JT, Kalmar K, Victor JD, Baker K, Gerber M, Fritz B, Eisenberg B, Biondi T, O'Connor J, Kobylarz EJ, Farris S, Machado a, McCagg C, Plum F, Fins JJ, Rezai a R (2007) Behavioural improvements with thalamic stimulation after severe traumatic brain injury. Nature 448:600–603.

Schmidt R, Leventhal DK, Mallet N, Chen F, Berke JD (2013) Canceling actions involves a race between basal ganglia pathways. Nat Neurosci 16:1118–1124.

Sherman SM, Guillery RW (1996) Functional organization of thalamocortical relays. 76:1367–95.

Sherman SM, Guillery RW (1998) On the actions that one nerve cell can have on another: distinguishing "drivers" from "modulators." 95:7121–6.

Sherman SM, Guillery RW (2001) Exploring the Thalamus. Academic Press.

Slézia A, Hangya B, Ulbert I, Acsády L (2011) Phase Advancement and Nucleus-Specific Timing of Thalamocortical Activity during Slow Cortical Oscillation. J Neurosci 31:607–617.

Somogyi P, Hodgson AJ, Chubb IW, Penke B, Erdei A (1985) Antisera to gamma-

aminobutyric acid. II. Immunocytochemical application to the central nervous system. 33:240–8.

Sunnemark D, Eltayeb S, Nilsson M, Wallström E, Lassmann H, Olsson T, Berg A-L, Ericsson-Dahlstrand A (2005) CX3CL1 (fractalkine) and CX3CR1 expression in myelin oligodendrocyte glycoprotein-induced experimental autoimmune encephalomyelitis: kinetics and cellular origin. J Neuroinflammation 2:17.

Thorn C a, Graybiel AM (2010) Pausing to regroup: thalamic gating of cortico-basal ganglia networks. Neuron 67:175–178.

Van der Werf YD, Witter MP, Groenewegen HJ (2002) The intralaminar and midline nuclei of the thalamus. Anatomical and functional evidence for participation in processes of arousal and awareness. Brain Res Brain Res Rev 39:107–140.

Wada E, Way J, Lebacq-Verheyden AM, Battey JF (1990) Neuromedin B and gastrin-releasing peptide mRNAs are differentially distributed in the rat nervous system. J Neurosci 10:2917–2930.

Walker AE (1938) The primate thalamus. Chicago: The University of Chicago Press.

Wojcik SM, Katsurabayashi S, Guillemin I, Friauf E, Rosenmund C, Brose N, Rhee J-S (2006) A shared vesicular carrier allows synaptic corelease of GABA and glycine. Neuron 50:575–587.

Zafra F, Aragón C, Olivares L, Danbolt NC, Giménez C, Storm-Mathisen J (1995) Glycine transporters are differentially expressed among CNS cells. J Neurosci 15:3952–3969.

Zeilhofer HU, Studler B, Arabadzisz D, Schweizer C, Ahmadi S, Layh B, Bösl MR, Fritschy J-M (2005) Glycinergic neurons expressing enhanced green fluorescent protein in bacterial artificial chromosome transgenic mice. J Comp Neurol 482:123–141.

Bibliography of the candidate's publications

Giber K[*], Diana MA[*], **M Plattner V[*]**, Dugué GP, Bokor H, Rousseau C V, Maglóczky Z, Havas L, Hangya B, Wildner H, Zeilhofer HU, Dieudonné S, Acsády L (2015) A subcortical inhibitory signal for behavioral arrest in the thalamus. Nat Neurosci 18:562–568.

Groh A, Bokor H, Mease R a, **Plattner VM**, Hangya B, Stroh A, Deschenes M, Acsády L (2013) Convergence of Cortical and Sensory Driver Inputs on Single Thalamocortical Cells. Cereb Cortex:1–13.

[*]equal contribution

Cumulated impact factor: 24.76

Acknowledgements

First of all, I would like to express my gratitude to Laci and Hajni for supervising my work and for their continuous support both during my undergraduate and PhD years.

I would also like to thank to all the people in the team for providing stimulating environment and for tolerating me during the agonizing months of the preparation of my thesis. I thank my co-authors in the papers, especially to Marco and Kristóf for working tirelessly and for their helpful questions and advices on the interpretation of my part in the work.

My sincere thanks also goes to Viktor Varga for his critical notes that helped me understand my results more deeply and to Mark Eyre for not only correcting my grammatical and stylistic errors but also for taking the time to bring little inconsistencies and additional literature about the topic to my attention.

Last but not least I would like to thank my family, my parents for being patient and open-minded enough to support my studies and my sister for always finding the time to talk with me.

List of Figures

Figure 1.2.1. Example of different projection patterns of various thalamic nuclei. 3
Figure 1.6.1. Glycinergic labelling in the midbrain of GlyT2::eGFP transgenic animals. 9
Figure 1.7.1. Distribution of drivers with different origin in the primate thalamus. 12
Figure 4.1.1. Retrograde labeling from the IL. 30
Figure 4.1.2. Validation of selective cre expression in the glycinergic neurons. 31
Figure 4.1.3. Anterograde virus tracing from the PRF in GlyT2::cre animals. 32
Figure 4.1.4. Distribution of glycinergic fibers in mouse and human. 33
Figure 4.1.5. Electronmicrographs of glycinergic terminals in mouse and human. 34
Figure 4.2.1. Electrode arrangement for juxtacellular recording in the PRF 35
Figure 4.2.2. Baseline activity of the PRF glycinergic neurons. 36
Figure 4.2.3. Phase coupling of eight recorded and identified glycinergic neurons. 37
Figure 4.2.4. Antidromic activation of a recorded PRF neuron from the thalamus. 39
Figure 4.3.1. Photostimulation-induced glycinergic inhibition of a tonically active IL thalamic neuron. 41
Figure 4.3.2. Photostimulation-induced glycinergic inhibition of a pain-sensitive IL thalamic neuron. 42
Figure 4.4.1. Electrode arrangement for the activation of the glycinergic fibers in the IL thalamus in freely behaving animals. 44
Figure 4.4.2. Behavioral effects of the photoactivation of glycinergic fibers. 45
Figure 4.4.3. Cortical activity during stimulation in freely behaving animals. 46
Figure 4.4.4. Power spectrum of the cortical LFP during stimulus and control. 47
Figure 4.5.1. Retrograde tracing from PRF. 49
Figure 4.5.2. Virus injection into frontal cortical motor areas in transgenic RBP4::cre/GlyT2::eGFP animals. 50
Figure 4.5.3. Transfected frontal cortical fibers in the PRF. 51
Figure 4.6.1. Spontaneous desynchronization of cortical activity. 52
Figure 4.6.2. Effect of cortical spreading depression (CSD) on PRF activity. 53
Figure 4.6.3. Effect of cortical inactivation on the firing rate of glycinergic cells. 54

Figure 4.7.1. Response of PRF cells to electrical stimulation of the cortex. 55
Figure 4.7.2. Optical activation of L5 pyramidal cells in a transgenic animal. 56
Figure 4.8.1. Somatosensory nuclei of the rodent thalamus. 58
Figure 4.8.2. Distribution of fibers with different origin in the POm at six rostro-caudal levels. 59
Figure 4.8.3. Putative zones of convergence in the POm of rat and mouse. 60
Figure 4.8.4. Distribution of the diameter of the dendritic domains targeted by drivers with different origin compared to randomly sampled terminals. 61
Figure 5.2.1. Thalamic and extrathalamic inhibitory systems 63
Figure 5.2.2. The nondepressing nature of the PRF – IL glycinergic synapse. 65
Figure 5.5.1. Evoked activity in POm neurons by co-occuring cortical and sensory signals. 68
Figure 6.2.1. IL neurons expressing the cre enzyme in the MR89-CRE mouse line 70